NASA Technical Memorandum 87035

Reliability of Void Detection in Structural Ceramics Using Scanning Laser Acoustic Microscopy

Don J. Roth, Stanley J. Klima,
and James D. Kiser
Lewis Research Center
Cleveland, Ohio

and

George Y. Baaklini
Cleveland State University
Cleveland, Ohio

Prepared for the
Spring Meeting of the American Society for
Nondestructive Testing
Washington, D.C., March 11-14, 1985

RELIABILITY OF VOID DETECTION IN STRUCTURAL CERAMICS USING SCANNING LASER ACOUSTIC MICROSCOPY

Don J. Roth, Stanley J. Klima, and James D. Kiser
National Aeronautics and Space Administration
Lewis Research Center
Cleveland, Ohio

and

George Y. Baaklini
Cleveland State University
Cleveland, Ohio

SUMMARY

The reliability of scanning laser acoustic microscopy (SLAM) for detecting surface voids in structural ceramic test specimens was statistically evaluated. Specimens of sintered silicon nitride and sintered silicon carbide, seeded with surface voids, were examined by SLAM at an ultrasonic frequency of 100 MHz in the as-fired condition and after surface polishing. It was observed that polishing substantially increased void detectability. Voids as small as 100 μm in diameter were detected in polished specimens with 0.90 probability at a 0.95 confidence level. In addition, inspection times were reduced up to a factor of 10 after polishing. The applicability of the SLAM technique for detection of naturally occurring flaws of similar dimensions to the seeded voids is discussed. A Fortran program listing is given for calculating and plotting flaw detection statistics.

E-2591

INTRODUCTION

Silicon nitride (Si_3N_4) and silicon carbide (SiC) ceramics are under investigation as candidate materials for hot-section components in advanced heat engines (refs. 1 to 5). Because these ceramics can withstand higher operating temperatures than their metallic counterparts, their use would result in significantly increased fuel efficiency. Presently, state-of-the-art structural ceramics exhibit wide variability in strength and low fracture toughness. These undesirable properties are generally attributed to flaws introduced during fabrication processes in the form of voids, microcracks, and foreign material inclusions (refs. 6 to 12). Flaws as small as 10 μm have been defined as critical; that is, potentially failure causing (refs. 6, 8, and 9).

Sensitive, reliable, nondestructive evaluation (NDE) techniques are needed to detect flaws in structural ceramics and reject parts containing critical flaws or concentrated flaw populations (refs 7, 8, and 13). NDE techniques can also aid in process optimization by identifying the stages of fabrication during which flaws are introduced (refs. 7, 13, and 14). Scanning laser acoustic microscopy (SLAM) is an attractive NDE technique because of its ability to image surface and subsurface microflaws in real time. It is applicable to densified ceramics, and has previously been shown to be capable of detecting critical flaws in Si_3N_4 and SiC specimens (refs. 5, 7, 9, 10, 15, and 16). To date, however, a complete statistically based evaluation of the reliability of SLAM for detecting failure-causing flaws in structural ceramics has not been accomplished.

This report describes a study that was conducted to evaluate the reliability of SLAM for detecting surface voids in sintered Si_3N_4 and sintered SiC specimens. The approach was to determine detection reliability for statistically significant populations of seeded surface voids in specially prepared laboratory specimens. The effects of specimen thickness and surface condition on void detectability were investigated. The applicability of the reliability results obtained for the seeded surface voids to naturally occurring internal and surface-connected flaws is discussed.

STATISTICAL RELIABILITY THEORY

The reliability of an NDE inspection technique is a quantitative measure of the ability of that technique to detect flaws of a specific type and size in a particular material. Reliability assessment is probabilistic in nature because inspection results are influenced by many variables. These variables include flaw shape and orientation, material surface texture and microstructure, and equipment and operator performance (ref. 17). Methods for analyzing the reliability of NDE inspection techniques are discussed in reference 18. This study was based on specimens containing seeded surface voids where the total number of seeded voids and their locations were known. Since an existing void was either detected or not detected (only two outcomes possible), SLAM reliability was determined by using binomial distribution statistics (refs. 17 and 19).

By using binomial distribution statistics, an initial estimate for the true (unknown) probability of detection of voids of diameter d can be taken as (ref. 17)

$$\bar{p} = \frac{S}{N} \tag{1}$$

where $\bar{p}$ is defined as a point estimate of true probability, S is the number of detected seeded surface voids of diameter d, and N is the total number of seeded surface voids of diameter d. There is an uncertainty associated with $\bar{p}$ because it is calculated for a relatively small number of inspections. Therefore, a conservative confidence level estimate of the true probability is preferred. This estimate is defined as the lower-bound probability p_ℓ. The lower-bound probability is considered an appropriate measure of the reliability of an NDE inspection technique (ref. 17) and is used in this study to describe the reliability of SLAM. A lower-bound probability (of detection) p_ℓ can be calculated from the following expression (ref. 17):

$$1 - G = \sum_{X=S}^{N} \left[\frac{N!}{X!\ (N - X)!}\right] (p_\ell)^X (1 - p_\ell)^{N-X} \tag{2}$$

where G is the selected confidence level.

A statistically significant probability of detection is 0.90 at a 0.95 confidence level (ref. 18). It is not sufficient just to have a high ratio of voids detected to voids seeded to obtain 0.90 probability of detection at a 0.95 confidence level using equation (2). Probability p_ℓ is also dependent on the quantity of voids seeded. For example, if 10 voids 100 μm in diameter are seeded and all are detected, the probability of detection of 100 μm voids is only 0.74 at a confidence level of 0.95. It is necessary to have 29 voids detected out of 29 voids seeded to obtain a probability of detection of 0.90. Further, 0.90 probability of detection at a 0.95 confidence level means that there is a 0.05 (1 - G) probability that 0.90 is an overestimate of the true probability of detection

MATERIALS AND PROCEDURES

In this study, specially prepared ceramic specimens seeded with surface voids were used to characterize the reliability of 100 MHz SLAM for detecting flaws in structural ceramic test specimens. Seeded surface voids (as opposed to another flaw type) were used because they could be easily identified (number and location) and accurately characterized (size and shape) by visual methods. This allowed the investigator to gather accurate flaw detection data during SLAM inspections. The specimens and voids were characterized using surface profiling instrumentation, metallography techniques, and optical and electron microscopy. SLAM inspection of the specimens in the as-fired condition and after polishing was performed, and data on void detectability were gathered. The inspection data were grouped according to void diameter and analyzed. Curves of probability of detection as a function of void diameter were generated.

Ceramic Specimen Development

Test specimens similar in composition to typical sintered Si_3N_4 and sintered SiC were fabricated with seeded surface voids. The starting materials were -100-mesh Si_3N_4 powder containing Y_2O_3 and SiO_2 sintering aids and -100-mesh alpha-SiC powder containing boron and carbonaceous resin binders. A selected amount of either powder was pressed in a double-action tungsten carbide (WC)-lined die at approximately 60 MPa to form a modulus-of-rupture (MOR) test bar. While still in the die, the bar was carefully dusted using a moisture-free aeroduster in order to remove excess powder from the top surface. Approximately 20 styrene divinylbenzene microspheres of the same size (115, 80, or 50 μm in diameter) were positioned on the top surface of the bar along the longitudinal axis. The test bar was then pressed at approximately 120 MPa, removed from the die, and once again dusted. With the microspheres now impressed into the test specimen surface, the specimen was vacuum sealed in thin-walled latex tubing and cold isopressed at 420 MPa.

The procedure was repeated to form all the green test specimens. Different bar thicknesses were obtained by using different amounts of powder. The seeded specimens were then heated to 525 °C under a vacuum and baked for 45 min to allow the polymer microspheres to decompose. A crater, or surface void, was left at each position on the specimen surface where a microsphere had been impressed. Following the vacuum heat treatment, the surface of each specimen was dusted to remove any remaining debris from the intentionally created surface voids (craters). Finally, the Si_3N_4 test specimens were sintered at 2140 °C under 5 MPa of nitrogen pressure for 2 hr. The SiC test specimens were sintered at 2200 °C under 0.1 MPa of argon pressure for 0.5 hr. The as-fired specimens were approximately 30 mm in length and 6 mm in width, while the thicknesses varied from approximately 2 to 4 mm.

After initial SLAM inspection of the specimens in the as-fired condition, the specimens were surface treated in the following manner: 23 sintered silicon nitride (SSN) specimens and 2 sintered silicon carbide (SSC) specimens were individually hand polished. The seeded void surface of each specimen was pressed against either 600-grit (for SSN) or 320-grit (for SSC) silicon carbide grinding paper attached to a rotating metallographic polishing wheel. The opposite surface of the specimen was not specially prepared in any way. The surface of a single SSN specimen was diamond ground using 400-grit diamond grinding paper. After surface treatment, all specimens were reinspected using SLAM.

Specimen and Void Characterization Techniques

The surface condition of several representative specimens of each material in the as-fired condition and after surface polishing was evaluated using a surface profile measuring system. The surface condition of the diamond-ground SSN specimen was also measured perpendicular to the grinding direction. The surface profiler used a diamond stylus, 12.5 μm in diameter, in contact with the surface of the specimen to measure the peak-to-valley roughness. A 2 mm length of the surface of each specimen was profiled. The maximum peak-to-valley roughness was obtained from each profile. To obtain information about the material microstructure, polished, unetched cross sections of representative SSN and SSC specimens were examined at a magnification of 200 by using a metallograph. Optical micrographs were acquired at different cross-sectional locations.

A photograph of the seeded void surface of each specimen was obtained at a magnification of 5 to aid in locating the voids during optical, electron, and acoustic microscopy. The location of each void was determined to the nearest 0.2 mm relative to an x-y coordinate system. Each void was then examined at a magnification of 200 by using the metallograph. The void diameter was measured using a calibrated reticle inserted into the metallograph. The depth of the void was measured by focusing first on the surface of the specimen near the void and then on the bottom of the void. Subtraction of one reading (of the calibrated graduations on the fine focus control) from the other gave the depth of the void. Optical micrographs of representative voids for each specimen were obtained. In order to investigate void morphology in more detail, several specimens were examined at a magnification of 400 to 450 using a scanning electron microscope (SEM). SEM micrographs of representative voids were acquired. Voids were characterized in as-fired specimens and after surface polishing.

Scanning Laser Acoustic Microscopy

Figure 1(a) shows a schematic diagram of the operation of the scanning laser acoustic microscope. The SLAM makes use of a laser to detect mechanical distortions (of the order of angstroms) produced on the surface of a specimen by piezotransducer-generated, high-frequency ultrasonic waves traveling through the specimen (ref. 9). In this manner, an acoustic picture of the specimen, including surface and subsurface defects such as voids, inclusions, and cracks, is obtained and displayed on a video monitor.

Figure 1(b) illustrates the experimental setup used when inspecting ceramic specimens on the SLAM. The specimen is placed on the SLAM stage over the piezoelectric transducer. A clear plastic coverslip, coated on one side with a thin (approximately 0.1 μm thick) film of gold, is placed on top of the specimen. The purpose of the metallized coverslip is to provide a mirrorlike reflective surface for the laser. Typically, the surface of the ceramic specimen is too rough to reflect light in a mirrorlike manner. Distilled water is used as a couplant between transducer and specimen and between specimen and coverslip. The transducer, located in a small well 0.5 mm below the stage surface, radiates continuous 100 MHz ultrasonic waves toward the specimen at an incident angle of 10°. The longitudinal ultrasonic waves are transmitted through the water couplant to the specimen surface, where they are refracted (based on Snell's law). Only the shear wave component, traveling at an angle of approximately 45° from the vertical, is utilized for SLAM inspection of SSN and SSC. The interaction of the shear waves with the top surface of the specimen sets up a ripple pattern on the top surface. The ripple is transmitted through the water couplant to the coverslip, where it sets up a corresponding ripple pattern on the gold film. The peaks of the ripple vary in amplitude according to the intensity of the ultrasonic waves producing them.

A laser beam constantly raster scans an approximately 2.0 by 2.3 mm area of the coverslip, is angularly modulated by the peaks of the ripple pattern, and is reflected to a photodetector. The photodetector converts the modulated laser light to an electronic signal. This signal is processed and used to create a real-time, black-and-white acoustic image that is displayed on a video monitor at a magnification of approximately 100. Generally, the brightest regions on the acoustic image represent areas of high acoustic transmission through the ceramic specimen while the darker regions correspond to areas of low or no acoustic transmission.

SLAM inspection of a specimen was performed with the surface containing the seeded voids nearest the laser. The specimen was positioned such that the specific void to be detected was located near the center of the laser spot. This procedure reduced the possibility of acoustic images of seeded voids being confused with acoustic images of naturally occurring flaws which were similar in appearance. The x-y coordinates of the voids, obtained from optical photographs of the specimen, were utilized in this procedure. Some specimens had to be rotated between 0° and 180° about the laser axis to obtain the best acoustic image. Some specimens were slightly warped, and the tilt controls on the SLAM stage had to be constantly adjusted to maintain the optimum acoustic image. Detection of a void was defined as the ability to discriminate the void from background noise (ref. 14) due to naturally occurring flaws and material artifacts. The time it took to inspect a specimen was noted and used as an index of difficulty in finding the seeded surface voids in that particular specimen. Acoustic micrographs of representative voids in each specimen were obtained.

Data Grouping and Analysis

At most discrete void diameters, an inadequate number of voids were experimentally produced to provide a valid statistical sample. Also, there was an error involved in measuring the actual void diameter. It would have been misleading, therefore, to calculate probability of detection for discrete void diameters. Instead, the voids were grouped into small (10 μm) intervals according to diameter, and the probability of detection was calculated over these intervals. The optimized-probability method (ref. 17) was used to further arrange the voids, because the number of voids in many 10-μm intervals was still insufficient for a valid statistical sample. This method increases the size of the sample used to calculate probability by including inspection data from intervals containing smaller flaws. Its use is justified by assuming that the probability of detection increases with increasing void diameter (ref. 17). Appendix A illustrates the use of the optimized-probability method to obtain the probability of detection results in this study. Appendix B lists a Fortran computer program for grouping the void detectability data, performing probability calculations, and plotting the results in the form of probability of detection (at a 0.95 confidence level) as a function of void diameter for each experimental data set.

RESULTS AND DISCUSSION

Specimen and Void Characterization

Table I indicates specimen surface condition, density, and size for each material. The specimens were similar in surface condition and density to typical sintered Si_3N_4 (SSN) and sintered SiC (SSC) MOR bars. The specimens were grouped into three discrete thickness ranges for SSN and two discrete thickness ranges for SSC. Throughout the remainder of this report, the SSN specimen thickness ranges 2.1 to 2.2, 2.9 to 3.2, and 3.8 to 4.1 mm are referred to as 2, 3, and 4 mm thicknesses, respectively. The SSC specimen thickness ranges 2.8 to 3.0 and 3.7 to 4.0 mm are referred to as 3 and 4 mm thicknesses, respectively.

Figures 2(a) to (e) show center and edge optical micrographs of unetched cross sections illustrating the variation of porosity within typical specimens. The pores are the dark spots in the micrographs. The porosity was uniform for SSC but varied from center to edge for SSN specimens. Porosity was greater at the center than near the edge for SSN.

Figure 3 shows an optical photograph of the seeded void surface of a typical test specimen. All the voids could be readily located from such photographs. Figure 4 shows optical micrographs of a typical seeded surface void in a test specimen in the as-fired condition and after polishing. In as-fired specimens, the error in the measurement of the void diameter using the metallograph was estimated at only ±5 μm because the void perimeter was essentially circular and readily definable. After polishing, the thickness of each bar was reduced by approximately 10 to 30 μm and the measured void diameter was increased by approximately 10 to 30 μm because of spalling at the void perimeter. The error in the diameter measurement after polishing was estimated at ±10 μm. In this case, void borders were jagged and hence more difficult to define than those in the as-fired specimens.

The diameter ranges of the seeded voids for each material, specimen thickness, and surface condition are shown in table I. Overall, the voids ranged from 40 to 165 μm in diameter. Figures 5(a) to (c) illustrate the typical morphology of the seeded surface voids. Figure 5(a) shows an electron micrograph of a typical seeded void in an as-fired specimen. Figures 5(b) and (c) are side-view diagrams illustrating the difference in shape between voids in SSN specimens and those in SSC specimens. From the diameter and depth data and electron micrographs, it was inferred that the voids were ellipsoidal rather than spherical. The voids in SSC specimens were generally shallower than those in SSN specimens.

SLAM Inspection of Specimens

Figures 6 and 7 show representative surface profiles and associated acoustic micrographs for SSN and SSC specimens, respectively, in the as-fired condition and after surface treatment. The acoustic micrographs (including the appearance of the detected voids) are typical for all specimen thicknesses examined. Ultrasonic wave interaction with the relatively large and random surface roughness typical of the as-fired specimen created small dark rings of interference that mottled the acoustic image for SSN or SSC specimens in the as-fired condition (see figs. 6(a) and (b) and 7(a) and (b)). The mottling masked the seeded surface voids making them difficult, if not impossible, to detect. Regardless of specimen thickness, the acoustic images of SSN and SSC specimens improved considerably after polishing only the surface containing the seeded voids (compare figs. 6(b) and (d) and 7(b) and (d)). Void detectability was substantially enhanced since only negligible interference was generated by the relatively small surface roughness typical of the polished specimens (see figs. 6(c) and 7(c)). (The residual surface roughness of the polished bars was attributed to numerous tiny imperfections on the surface as a result of incomplete polishing. These imperfections are evident in the acoustic image of the polished SSN specimen (see fig. 6(d)) and are an indication of the sensitivity of 100 MHz SLAM. The optimally polished areas of the specimens had a mirrorlike surface finish.) Many of the voids not detected during inspection of the as-fired specimens were detected after polishing, while those originally detected in the as-fired specimens were much more easily detected after polishing. Individual specimen inspection times were up to an order of magnitude shorter after polishing because of the improved void detectability. Typical inspection times for as-fired and polished specimens were 50 min and 5 min, respectively.

Figure 6(e) shows the surface profile of the diamond-ground SSN specimen taken perpendicular to the grinding direction. The diamond-ground surface is visibly smoother than the as-fired surface but contains periodic roughness greater than the random roughness in the hand-polished surfaces (compare figs. 6(c) and (e)). The acoustic image of the diamond-ground specimen, however, is similar in clarity to that of the hand-polished specimen despite the presence of striations produced by grinding marks (compare figs. 6(d) and (f)). It is believed that the latter result is due to the fact that the roughness (grinding marks) of the diamond-ground specimen is ordered and uniform as well as low (as compared to that of the as-fired surface). It is obvious from the previously mentioned figures that void detectability is directly related to acoustic image quality. Therefore, results similar to those obtained for the hand-polished bars might be expected for diamond-ground MOR bars which are used in structural ceramic development and evaluation.

It should be noted that, in general, the acoustic image of as-fired SSC specimens were slightly clearer than that of as-fired SSN specimens (compare figs. 6(b) and 7(b)). Hence, the voids were generally easier to detect in as-fired SSC than in as-fired SSN. The reason for this is unclear, but it is likely to be due to differences in surface topology and specimen microstructure between the as-fired materials. Although distinct topological differences were not apparent from the profile measurements, it is possible that microscopic differences could exist on the surface of the materials. Moreover, it is felt that the SSN, because of its variable pore distribution (see figs. 2(b) and (c)), may have been a more attenuating material than the SSC. A difference in acoustic image with specimen thickness was noted only for the as-fired SSN specimens. In this case, the acoustic images of the 2 and 3 mm thick specimens appeared slightly clearer than the images of the 4 mm thick specimens.

Reliability of Void Detection

The seeded void detectability data obtained using SLAM is presented in table I. These data are presented in raw form for each material, specimen thickness, and surface condition in the void size distribution plots of appendix C. Figures 8 to 10, derived from the raw data given in appendix C, show the statistical reliability of SLAM in the form of probability of detection (at a 0.95 confidence level) as a function of void diameter (POD) curves.

It is important to note two competing factors that may have biased the POD curves. First, the locations of all seeded voids were known, and each test specimen was examined carefully at these locations. Though essential to establishing probability of detection statistics, this procedure biased the detection probabilities toward higher-than-normal values since neither the number nor the location of flaws is known during normal part inspections. A second factor, on the other hand, is the fact that although the optimized-probability method of data grouping increases the size of the sample used in calcualting a probability value, the value obtained is conservative because it includes data from smaller voids. Each point on the POD curves corresponds to the largest void diameter contained in the interval over which probability was calculated. Although a POD curve can be plotted through the midpoints of the void diameter intervals, the conservative approach of reference 17 is preferred to minimize the bias resulting from prior knowledge of void location.

Figures 8(a) to (c) show POD curves for the seeded voids in as-fired and polished SSN specimens of thickness 4, 3, and 2 mm, respectively. These figures illustrate the improvement in void detectability after polishing. For the as-fired specimens of any thickness, no voids of any diameter were detected with 0.90 probability. Overall, only 45 percent of the voids examined in the as-fired SSN specimens were detected (129 voids detected out of 284 voids examined). After polishing, voids as small as 100 to 150 μm in diameter were detected with at least 0.90 probability. (The smallest void diameter at which 0.90 probability of detection occurred was different for each specimen thickness.) Had a sufficient number of voids (large enough statistical sample) been seeded in the 50 to 100 μm diameter range, it is felt that voids in this range would have been detected with at least 0.90 probability as well. Overall, 97 percent of the surface voids examined in the polished SSN specimens were detected (262 voids detected out of 270 voids examined). Some of the SSN test specimens were slightly warped making uniform polishing difficult. As a result, small areas of the surface of a warped bar remained with the as-fired roughness. The acoustic image in these areas was mottled and void detection was difficult. Voids undetected as a result of the mottling caused the curve labeled "polished" in figure 8(a) to dip below 0.90 probability at void diameters between 85 and 125 μm. If the polishing had been uniform, it is likely that all of the seeded voids would have been detected.

Figures 9(a) and (b) show POD curves for the seeded voids in as-fired SSC specimens for the 4 and 3 mm specimen thicknesses, respectively. Voids as small as 100 to 150 μm in diameter were detected with a least 0.90 probability. (The smallest void diameter at which 0.90 probability of detection occurred was different for each specimen thickness.) Overall, 88 percent of the voids examined in the as-fired SSC specimens were detected (306 voids detected out of 346 voids examined).

As discussed previously, the acoustic image of as-fired SSC specimens was slightly less mottled than that of as-fired SSN specimens. Hence, better POD results were obtained for as-fired SSC than for as-fired SSN. Detection of voids was still difficult, however, and inspections for individual as-fired SSC specimens were approximately as lengthy as those for as-fired SSN specimens (up to 60 min). If the inspection time for individual as-fired SSC specimens had been limited to that recorded for individual polished specimens, the POD results would have been much poorer. Only representative SSC specimens were polished because polishing would not significantly improve POD results for SSC specimens (most voids in the as-fired SSC specimens were found). Therefore, statistical data are not available for polished SSC specimens. To illustrate typical inspection results for polished SSC, a SSC specimen seeded with 13 surface voids was inspected in the as-fired condition and after polishing. In the as-fired condition, 10 voids were detected out of 13 examined in an inspection taking 45 min. After polishing, 13 voids were detected out of 13 examined in an inspection taking 5 min.

Figures 10(a) to (c) show the POD curves of figures 8 and 9 organized to illustrate the effect of specimen thickness on void detectability for each material. Since a difference in the acoustic image with specimen thickness was noted only for the as-fired SSN specimens (clearer acoustic image for thinner specimens), POD noticeably varied with thickness only in this case (compare figs. 10(a) to (c)). As shown in figure 10(a), better POD results were obtained the thinner the as-fired SSN specimen. POD did not appear to be a function of specimen thickness for polished SSN or as-fired SSC specimens (for the thicknesses investigated) since the respective acoustic image of each material did not change noticeably with thickness. If similar void diameter distributions had been available for each specimen thickness for the polished SSN and as-fired SSC, the POD curves within figures 10(b) and (c) would be expected to be nearly identical.

The detectability results presented for seeded voids in SSN and SSC specimens indicate that reliability of void detection and ease of inspection are directly related to acoustic image quality. Since acoustic image quality is highly dependent on specimen surface condition, present as-fired specimens of SSN and SSC need an improved surface condition if they are to be inspected for flaws in a time-efficient and reliable manner using SLAM.

In this study, only artificially seeded voids in polished SSN specimens were detected with 0.90 probability at a 0.95 confidence level. It is believed, however, that this result can be extended to naturally occurring surface and near-surface flaws in smoothly ground structural ceramic test specimens. (For purposes of discussion, a near-surface flaw is arbitrarily defined as one that is not surface connected but is wholly contained within two lengths of the surface.) To illustrate, figure 11 shows acoustic images of three naturally occurring flaws in a diamond-ground silicon nitride specimen (ref. 7). Flaw A is a surface-connected inclusion, and flaw B is a surface-connected crack-like defect. Flaw C is a near-surface defect having a crack-like appearance. Each flaw is near 100 μm in either length or width. As was the case for almost all seeded voids in polished SSN and SSC specimens, flaws A, B, and C were readily detected because of the clarity of the acoustic image. Hence, flaws in this size range in diamond-ground structural ceramic test specimens would be expected to be detected with 0.90 probability at a 0.95 confidence level. It is worth noting that while SLAM imaged all three flaws in figure 11, flaw B could not be resolved by radiographic methods and flaw C could not be resolved by radiographic or optical methods.

CONCLUSIONS

Scanning laser acoustic microscopy was determined to be a time-efficient, statistically reliable technique for detecting surface-connected voids in structural ceramic specimens with smooth surfaces. Surface voids as small as 100 μm in diameter in polished sintered silicon nitride specimens were detected with 0.90 probability at a 0.95 confidence level. Similar detection reliabilities were not achieved for voids in as-fired sintered silicon nitride specimens that exhibit rough surfaces. Additionally, inspection time was reduced up to a factor of 10 after as-fired surfaces were polished. Seeded surface voids were used to establish reliability of detection statistics in this investigation because they could be accurately characterized in terms of their size and shape using visual techniques. Evidence was presented, however, showing that the detectability of surface-connected and near-surface flaws in specimens with diamond-ground surfaces may be similar to the detectability obtained for the voids in the polished specimens. Hence, it was inferred that the detection reliabilities reported herein are applicable to surface and near-surface flaws in smoothly ground specimens.

APPENDIX A

OPTIMIZED-PROBABILITY METHOD OF DATA GROUPING

Table II shows a sample set of inspection data arranged in (approximately) 10 μm intervals. The intervals were set so that each void appeared in only one interval. The steps of the optimized-probability method of data grouping to obtain probability of detection results from this data are illustrated in figure 12(a). The results are displayed as a plot of probability of detection (at a 0.95 confidence level) as a function of void diameter (fig. 12(b)). Note that each point on the plot corresponds to the largest void diameter contained in the interval over which probability of detection was calculated. Hence, although the size of the statistical sample was increased, the calculated probability of detection was conservatively influenced by the inspection results from smaller voids. The optimized-probability method demands great computational effort, but its use is necessary to overcome the problem of insufficient sample size.

APPENDIX B

FORTRAN COMPUTER PROGRAM LISTING

A Fortran computer program that calculates and plots NDE flaw inspection reliability is listed in this appendix. The program was written for a Digital PDP 11/45 minicomputer interfaced with a Grinnell 274 image processor. Its task file requires 64 kilobytes (125 blocks) of auxiliary memory. Initially, flaw inspection data (the number and size of flaws examined and detected (see table II) is entered into the computer and stored in files (or retrieved if already stored). This data is arranged in intervals by using the options of equal flaw size interval, overlapping flaw size interval, or optimized probability methods (ref. 17). The user selects the interval sizes and method of data grouping. During the grouping, a record of the number and size of flaws examined and detected per interval is stored. The probability of detection p_ℓ is then calculated (ref. 20) over the range of flaw size data using any preselected confidence level. Two types of plots displaying quantitative flaw detectability results are generated on a video monitor using the image processor software routines. One plot shows the number of flaws examined and detected as a function of flaw size or flaw size/part thickness (see figs. 13 to 20, appendix C). The second plot shows the probability of detection p_ℓ (at the selected confidence level) as a function of flaw size or flaw size/part thickness (see figs. 8 to 10).

CALCULATION AND PLOTTING OF NDE FLAW

INSPECTION RELIABILITY

Don J. Roth
August, 1984

```
      INTEGER Z,Y,X,JR(200),LX,LR(100),LB(350),KB(350),XYDATA(500)
     1,XYDAT(500),LLBN(100),LLLBN(100),LLJZ3(100)
      BYTE ICHAR(2),IFLDAT(20)
      DIMENSION IIQ(300),KKQ(300),AR11(300),LLR(300),IXQ(300),KXQ(300)
      CHARACTER*8 J1,J2*25,J3*2,J4*4,J5*26,J11*5,J22*13,J33*10
     1,J44*20,J6*20,J50*1,J51*2,J52*2,J53*2,J54*2,J55*2,J56*2
     1,J57*2,J58*2,J59*2,J60*3,J61*3,J62*3,J63*3,J64*3,J65*3
     1,J66*3,J67*3,J68*3,J69*3,J70*3,J111*17,J112*21,J113*14
     1,J114*20,J115*21,J7*28,J71*1,J72*2,J73*2,J74*3
     1,J75*3,J76*3,J77*3,J78*3,J79*3,J80*3,J81*3,J82*3,J83*3
     1,J84*3,J85*3,J86*3,J87*3,J88*3,J89*3,J90*3,J91*3,J500*11
     1,J501*1,J502*2,J503*2,J900*16,J504*5,J505*5
C
C
      J11='DATE!'
      J22='SAMPLES I.D.!'
      J33='# SCANNED!'
      J44='AVE. THICKNESS (MM)!'
      J5='% NOITCETED FO YTILIBABORP'
      J6='FLAW SIZE (MICRONS)'
      J7='THICKNESS SENSITIVITY (*100)'
      J111='CONFIDENCE LEVEL!'
      J112='DATA GROUPING METHOD!'
      J113='EQUAL INTERVAL'
      J114='OVERLAPPING INTERVAL'
      J115='OPTIMIZED PROBABILITY'
      J500='SWALF FO # '
      J504='LATOT'
      J505='DNUOF'
      J900='FL. FREQ. DISTR.'
      DATA J50/'0'/J51/'10'/J52/'20'/J53/'30'/J54/'40'/J55/'50'/
     1J56/'60'/J57/'70'/J58/'80'/J59/'90'/J60/'100'/J61/'110'/
     1J62/'120'/J63/'130'/J64/'140'/J65/'150'/J66/'160'/J67/'170'/
     1J68/'180'/J69/'190'/J70/'200'/J71/'0'/J72/'25'/J73/'50'/J74/'75'/
     1J75/'100'/J76/'125'/J77/'150'/J78/'175'/J79/'200'/J80/'225'/
     1J81/'250'/J82/'275'/J83/'300'/J84/'325'/J85/'350'/J86/'375'/
     1J87/'400'/J88/'425'/J89/'450'/J90/'475'/J91/'500'/J501/'5'/
     1J502/'15'/J503/'25'/
C
      DATA LMX/0/LL,,X/0/MMM/1)00/N99/1000/
      DATA IFLDAT/'D','M','O',':','E','1',',','5','4','J',
     1' ',' ',' ',' ',' ',' ','.','D','A','T'/
C
C              INITIALIZE GRINNELL HARDWARE & SOFTWARE
C
      CALL GRINIT
      CALL GRSINI
      CALL GRSRST
      CALL GRSBFI (0)
      CALL GRFER (4095,4095,0)   !ERASE EVERYTHING ON VIDEO
C
      CALL GRNIN (1,0,0,0)     !CHANNEL 0 TO ALL LOOKUP TABLES
```

```
      CALL GRNBY (1,1,1,1)     !BYPASS ALL LOOKUP TABLES
C
      TYPE *,'----------------------------------------'
      TYPE *,'    '
      TYPE *,'  ENTER TODAYS DATE (I.E. 12/11/54)!'
      READ (5,598) J1
  598 FORMAT (A8)
      K1=LEN(J1)        !OBTAIN LENGTH OF DATE
      TYPE *,'    '
      TYPE *,'  ENTER I.D. OF SAMPLES (EX. AF-SIC-4)!'
      READ (5,601) J2
  601 FORMAT (A25)
      K2=LEN(J2)        !OBTAIN LENGTH OF I.D.
      TYPE *,'     '
      TYPE *,'  ENTER # OF SAMPLES SCANNED!'
      READ (5,602) J3
  602 FORMAT (A2)
      K3=LEN(J3)        !OBTAIN LENGTH OF # #
      TYPE *,'     '
      TYPE *,'  ENTER AVERAGE THICKNESS OF SAMPLES IN MM!'
      READ (5,603) J4
  603 FORMAT (A4)
      K4=LEN(J4)        !OBTAIN LENGTH OF THICKNESS #
      TYPE *,'------------------------------------------------'
C
C
C
  611 TYPE *,'    '
      TYPE *,'    ENTER DATA GROUPING METHOD!'
      TYPE *,'  0 - EQUAL INTERVAL (0% OVERLAP) POD'
      TYPE *,'  1 - OVERLAPPING INTERVAL POD'
      TYPE *,'  2 - OPTIMIZED PROBABILITY POD'
      TYPE *,'  3 - FLAW FREQUENCY DISTRIBUTION ONLY'
      READ (5,604) L99
  604 FORMAT(I1)
      TYPE *,'-------------------------------------------'
      IF (L99.GT.3) GOTO 611
      IF (L99.EQ.3) GOTO 2153        !# OF FLAWS PLOT
      IF (MMM.NE.1000) GOTO 2178 !PROCEED W/ANOTHER GROUPING METHOD
C
C
  629 TYPE *,'  ENTER CONFIDENCE LEVEL (%) DESIRED FOR P.O.D.'
      TYPE *,'                CALCULATION (EX. 95)'
      READ (5,39) IAR3
   39 FORMAT (I2)
      TYPE *,'-----------------------------------------------'
C
C              THE FOLLOWING IS A ROUTINE FOR CHANGING INTEGER
C              DATA (CONFIDENCE LEVEL, IAR3) TO CHARACTER DATA
C              SO IT CAN BE PRINTED OUT ON VIDEO VIA GRINNELL.
C              FOR DETAILED EXPLANATION OF HOW ROUTINE ACCOMPLISHES
C              THIS, SEE RBOX PROGRAM.
C
      ITEMP=IAR3
      RIAR3=FLOATI(IAR3)
      IE=INT(ALOG10(RIAR3))
      ICNT=1
      DO 2150 IF=0,IE
      IG=IE-IF
      ITEM=ITEMP/10**IG
      ICHAR(ICNT)=ITEM+48
```

```
      ITEMP=ITEMP-ITEM*10**IG
      ICNT=ICNT+1
 2150 CONTINUE
      ICNT=ICNT-1
      IF (MMM.NE.1000) GOTO 2178  !PROCEED W/NEW CONFIDENCE LEVEL
C
C
 2153 TYPE *,'          ENTER!'
      TYPE *,'  0 - TO ANALYZE RADIOGRAPHY DATA'
      TYPE *,' ANY OTHER # - TO ANALYZE SLAM DATA'
      READ (5,2157) L32
 2157 FORMAT (I1)
      TYPE *,'-----------------------------------------------'
C
C
C         THE FOLLOWING ARE GRINNELL MEMORY FILL ROUTINES
C         FOR THE P.O.D. VS. FLAW SIZE PLOT TO BE PRINTED
C         OUT ON VIDEO
C
 2178 CALL GRFER (4095,4095,0)
      CALL GRNIV (1,1,1,1)  !INVERT GRAPH COLORS
      CALL GRFCD (1,255,0,0,J22,10,470,6,0,13,0,0,0)  !SAMPLE I.D.
      CALL GRFCDS (1,255,J2,85,470,6,0,K2)    !SAMPLE I.D.
      CALL GRFCDS (1,255,J33,10,460,6,0,10)   !# OF SAMPLES
      CALL GRFCDS (1,255,J3,80,460,6,0,K3)    !# OF SAMPLES
      CALL GRFCDS (1,255,J44,45+K2*6,470,6,0,20)  !THICKNESS
 2179 CALL GRFCDS (1,255,J4,170+K2*6,470,6,0,K4)  !THICKNESS
      IF (N99.NE.1000) GOTO 352     !RETURN TO DATA RETRIEVAL ROUTINE
      CALL GRFCDS (1,255,J11,202+K2*6+K4*6,470,6,0,5) !DATE
      CALL GRFCDS (1,255.J1,242+K2*6+K4*6,470,6,0,K1) !DATE
      IF (MMM.EQ.3.OR.L99.EQ.3) GOTO 2985    !# OF FLAWS ON Y-AXIS
      CALL GRFCDS (1,255,J5,10,100,0,9,26)    !P.O.D
      GOTO 2987
 2985 CALL GRFCDS (1,255,J500,10,150,0,9,11)    !# OF FLAWS
      CALL GRFCDS (1,100,J504,5,250,0,9,5)  !TOTAL
      CALL GRFARS (1,100,6,310,3,20)  !TOTAL-DISPLAY COLOR
      CALL GRFCDS (1,255,J505,15,250,0,9,5) !FOUND
      CALL GRFARS (1,255,16,310,3,20)  !FOUND-DISPLAY COLOR
 2987 IF (L32.EQ.0) GOTO 2180  !RADIOGRAPHY
      CALL GRFCDS (1,255,J6,200,10,6,0,20)    !FLAW SIZE
      GOTO 2181
 2180 CALL GRFCDS (1,255,J7,200,10,6,0,28)  !THICKNESS SENSITIVITY
 2181 CALL GRFCDS (1,255,J111,100,460,6,0,17)     !CONFIDENCE LEVEL
      IF (L99.EQ.3) GOTO 2281
      CALL GRFCDS (1,255,ICHAR,206,460,6,0,ICNT) !CONFIDENCE LEVEL
C
 2281 CALL GRFCDS (1,255,J112,240,460,6,0,21)    !DATA GR. METHOD
      IF (L99.EQ.0) GOTO 686      !EQ. INT.
      IF (L99.EQ.1) GOTO 687    !OVERL. INT.
      IF (L99.EQ.3) GOTO 786     !# OF FLAWS PLOT
      CALL GRFCDS (1,255,J115,380,460,6,0,21) !OPT. PROB.
      GOTO 688
  686 CALL GRFCDS (1,255,J113,380,460,6,0,14) !EQ. INT.
      GOTO 688
  687 CALL GRFCDS (1,255,J114,380,460,6,0,20) !OVERL. INT.
      GOTO 688
  786 CALL GRFCDS (1,255,J900,380,460,6,0,16)     !# OF FLAWS PL.
C
  688 CALL GRFVC (1,255,0,0,50,50,450,50)  !X-AXIS
      CALL GRFVCS (1,255,50,50,50,450)    !Y-AXIS
C
```

```
      IF (MMM.EQ.3.OR.L99.EQ.3) GOTO 689    !# OF FLAWS PLOT
      GOTO 6161     !PROBABILITY PLOT
  689 DO 6121 I19=50,150,16       !# OF FLAWS PLOT Y HASH MARKS
      CALL GRFVCS (1 255,45,I19,50,I19)
 6121 CONTINUE
      IF (L32.EQ.0) GOTO 6026  !RADIO. F'. FREQ. X-AXIX HASH
      GOTO 6311      !X-AXIS HASH MARKS FLR SLAM FL. FR. PL.
C
 6161 DO 625 I19=50,450,8
      CALL GRFVCS (1,255,45,I19,50,I19)  !Y-AXIS (SMALL) HASH MARKS
  625 CONTINUE
      DO 6025 I22=50,450,40
      CALL GRFVCS (1,255,40,I22,50,I22)  !Y-AXIS (LARGE) HASH MARKS
 6025 CONTINUE
      IF (L32.EQ.0) GOTO 6026     !RADIOG.
 6311 INCR1=10      !FLAW SIZE HASH MARKS
      INCR2=20      !DITTO
      GOTO 6131
 6026 INCR1=8    !THICKNESS SENSITIVITY HASH MARKS/RADIO.
      INCR2=40   !DITTO
 6131 DO 626 I20=50,450,INCR1
      CALL GRFVCS (1,255,I20,45,I20,50)   !X-AXIS (SMALL) HASH MARKS
  626 CONTINUE
      DO 627 I21=50,450,INCR2
      CALL GRFVCS (1,255,I21,40,I21,50)   !X-AXIS (LARGE) HASH MARKS
  627 CONTINUE
      IF (MMM.EQ.3.OR.L99.EQ.3) GOTO 3864   !# OF FLAWS PLOT
C
C
      CALL GRFCDS (1,255,J50,35,50,6,0,1)   !Y-AXIS #'S
      CALL GRFCDS (1,255,J51,30,90,6,0,2)
      CALL GRFCDS (1,255,J52,30,130,6,0,2)
      CALL GRFCDS (1,255,J53,30,170,6,0,2)
      CALL GRFCDS (1,255,J54,30,210,6,0,2)
      CALL GRFCDS (1,255,J55,30,250,6,0,2)
      CALL GRFCDS (1,255,J56,30,290,6,0,2)
      CALL GRFCDS (1,255,J57,30,330,6,0,2)
      CALL GRFCDS (1,255,J58,30,370,6,0,2)
      CALL GRFCDS (1,255,J59,30,410,6,0,2)
      CALL GRFCDS (1,255,J60,25,450,6,0,3)
      CALL GRSBFD
      GOTO 3865
 3864 CALL GRFCDS (1,255,J50,35,50,6,0,1)      !# OF FLAWS Y-AXIS #'S
      CALL GRFCDS (1,255,J501,35,130,6,0,1)
      CALL GRFCDS (1,255,J51,30,210,6,0,2)
      CALL GRFCDS (1,255,J502,30,290,6,0,2)
      CALL GRFCDS (1,255,J52,30,370,6,0,2)
      CALL GRFCDS (1,255,J503,30,450,6,0,2)
      CALL GRSBFD
 3865 IF (L32.EQ.0) GOTO 628     !RADIOGRAPHY
C
      CALL GRFCDS (1,255,J50,50,30,6,0,1)   !X-AXIS #'S
      CALL GRFCDS (1,255,J51,65,30,6,0,2)
      CALL GRFCDS (1,255,J52,85,30,6,0,2)
      CALL GRFCDS (1,255,J53,105,30,6,0,2)
      CALL GRFCDS (1,255,J54,125,30,6,0,2)
      CALL GRFCDS (1,255,J55,145,30,6,0,2)
      CALL GRFCDS (1,255,J56,165,30,6,0,2)
      CALL GRFCDS (1,255,J57,185,30,6,0,2)
      CALL GRFCDS (1,255,J58,205,30,6,0,2)
      CALL GRFCDS (1,255,J59,225,30,6,0,2)
```

ORIGINAL PAGE IS
OF POOR QUALITY

```
      CALL GRFCDS (1,255,J60,242,30,6,0,3)
      CALL GRFCDS (1,255,J61,262,30,6,0,3)
      CALL GRFCDS (1,255,J62,282,30,6,0,3)
      CALL GRFCDS (1,255,J63,302,30,6,0,3)
      CALL GRFCDS (1,255,J64,322,30,6,0,3)
      CALL GRFCDS (1,255,J65,342,30,6,0,3)
      CALL GRFCDS (1,255,J66,362,30,6,0,3)
      CALL GRFCDS (1,255,J67,382,30,6,0,3)
      CALL GRFCDS (1,255,J68,402,30,6,0,3)
      CALL GRFCDS (1,255,J69,422,30,6,0,3)
      CALL GRFCDS (1,255,J70,442,30,6,0,3)
      CALL GRSBFD
      GOTO 59
C
  628 CALL GRFCDS (1,255,J71,50,30,6,0,1)   !RADIOGRAPHY X-AXIS #'S
      CALL GRFCDS (1,255,J73,85,30,6,0,2)
      CALL GRFCDS (1,255,J75,122,30,6,0,3)
      CALL GRFCDS (1,255,J77,162,30,6,0,3)
      CALL GRFCDS (1,255,J79,202,30,6,0,3)
      CALL GRFCDS (1,255,J81,242,30,6,0,3)
      CALL GRFCDS (1,255,J83,282,30,6,0,3)
      CALL GRFCDS (1,255,J85,322,30,6,0,3)
      CALL GRFCDS (1,255,J87,362,30,6,0,3)
      CALL GRFCDS (1,255,J89,402,30,6,0,3)
      CALL GRFCDS (1,255,J91,442,30,6,0,3)
      CALL GRSBFD
C
   59 IF (MMM.EQ.0.AND.L99.EQ.0) GOTO 219   !EQ. INT. PATH
      IF (MMM.EQ.0.AND.L99.EQ.1) GOTO 219   !OVERL. INT. PATH
      IF (MMM.EQ.1.AND.L99.EQ.2) GOTO 6001  !OPT. PROB. PATH
      IF (MMM.EQ.2.AND.L99.EQ.2) GOTO 2005  !OPT. PROB. PATH
      IF (MMM.EQ.0.AND.L99.EQ.2) GOTO 2005  !OPT. PROB. PATH
      IF (MMM.EQ.1.AND.L99.EQ.0) GOTO 500   !EQ. INT. PATH
      IF (MMM.EQ.1.AND.L99.EQ.1) GOTO 500   !OVERL. INT. PATH
      IF (MMM.EQ.2.AND.L99.EQ.0) GOTO 219   !EQ. INT. PATH
      IF (MMM.EQ.2.AND.L99.EQ.1) GOTO 219   !OVERL. INT. PATH
      IF (MMM.EQ.3) GOTO 6028     !# OF FLAWS PLOT

          INITIALIZE FLAW SIZE DATA ARRAYS

      DO 61 MB=1,600
      XYDATA(MB)=0
      XYDAT(MB)=0
   61 CONTINUE
      DO 8 MB=1,300
      LB(MB)=0
      KB(MB)=0
    8 CONTINUE


      TYPE *,'        '
      TYPE *,'                 ENTER:'
      TYPE *,'  0 - TO ENTER NEW FLAW SIZE DATA'
      TYPE *,'  1 - TO RETRIEVE STORED FLAW SIZE DATA'
      READ (5,343) N99
  343 FORMAT (I1)
      TYPE *,'-----------------------------------------------------'
      IF (N99.EQ.0) GOTO 378      !ENTER NEW FLAW SIZE DATA


          THE FOLLOWING ROUTINE RETRIEVES FLAW SIZE DATA FROM DISK;
```

```
C          (FOR DETAILED DOCUMENTATION OF STORING AND RETRIEVING DATA,
C          SEE RBOX PROGRAM)
C
      TYPE *,'         '
      TYPE *,' TYPE IN THE 6-CHARACTER NAME OF DATA FILE YOU WISH'
      TYPE *,' TO RETRIEVE; (IF YOU INPUT O[ZERO], RETRIEVAL WILL BE'
      TYPE *,' ABORTED AND PROGRAM WILL PROCEED W/NEW DATA ENTRY'
      ACCEPT 350,IFLDAT(11),IFLDAT(12),IFLDAT(13),IFLDAT(14),
     1IFLDAT(15),IFLDAT(16)
  350 FORMAT (6A1)
      TYPE *,'-----------------------------------------------------------'
      IF (IFLDAT(11).EQ.'0') GOTO 378
      OPEN (UNIT=4,NAME=IFLDAT,STATUS='OLD',FORM='UNFORMATTED',
     1       BLOCKSIZE=1024)
C
C           RETRIEVE FLAW DATA FORM DISK
C
      READ (UNIT=4) J4,IB,LB,KB,NAN,LLBN,LLJZ3,LLLBN
      CLOSE (4)
      GOTO 2179       !TO PRINT THICKNESS ON VIDEO
  352 TYPE *,'-------------------------------------------'
      TYPE *,'             ENTER:'
      TYPE *,'  0 - WRITE OUT FLAW SIZE FILE DATA FILE TO TERMINAL'
      TYPE *,'  ANY OTHER # - DO NOT WRITE FILE TO TERMINAL'
      READ (5,3052) IJIJ
 3052 FORMAT (I1)
      IF (IJIJ.NE.0) GOTO 464
      WRITE (5,355) IFLDAT,IB
  355 FORMAT (10X,20A1,5X,I3,1X,'ENTRIES')
      TYPE *,'  '
      DO 353 N86=1,IB
      WRITE (5,354) N86,LB(N86),KB(N86)
  354 FORMAT (10X,'ENTRY(',I3,')',2X,I3,1X,I1)
  353 CONTINUE
C
C
C
 3332 TYPE *,'----------------------------------------------------'
      TYPE *,'DO YOU WISH TO CHANGE FLAW SIZE DATA FILE?'
      TYPE *,'                 ENTER:'
      TYPE *,'   0 - CHANGE AN ENTRY'
      TYPE *,'   1 - ADD ENTRIES TO FILE (FIRST CHANGE '
      TYPE *,'       LAST ENTRY [0000] OF ORIGINAL FILE'
      TYPE *,'       TO FIRST NEW ENTRY)'
      TYPE *,'   ANY OTHER # - NO CHANGE'
      READ (5,3333) NONO
 3333 FORMAT (I1)
      IF (NONO.GT.1) GOTO 464      !NO CHANGE
      IF (NONO.EQ.1) GOTO 3884     !ADD ENTRIES
C
C
      TYPE *,'         '
      TYPE *,'  ENTER # OF ENTRY YOU WISH TO CHANGE (I3 FORMAT)'
      READ (5,3335) JIB
 3335 FORMAT (I3)
      WRITE (5,3336) JIB,LB(JIB),KB(JIB)
 3336 FORMAT (1X,'FLAW SIZE #',1X,I3,'=',1X,I3,1X,I1)
      TYPE *,'     '
      TYPE *,'        ENTER:'
      TYPE *,' 0000 - TO DELETE FLAW SIZE ENTRY'
      TYPE *,' I3,I1 # - REPLACEMENT FLAW SIZE ENTRY'
```

```
      READ (5,3337) LB(JIB),KB(JIB)
 3337 FORMAT (I3,I1)
      GOTO 3993
C
C
 3884 TYPE *,'   ENTER # OF NEW ENTRIES YOU WISH TO ADD TO FILE'
      TYPE *,'   (NOTE:   0000 MUST BE INCLUDED AS FINAL ENTRY)'
      READ (5,3885) IBP
 3885 FORMAT (I3)
      DO 3886 NET=1,IBP
      WRITE (5,3887) NET
 3887 FORMAT (5X,'ENTRY #',1X,I3,1X,'=(I3,I1 FORMAT)')
      READ (5,3888) LB(IB+NET),KB(IB+NET)
 3888 FORMAT (I3,I1)
 3886 CONTINUE
      IB=IB+IBP
      TYPE *,'         '
 3993 OPEN (UNIT=4,NAME=IFLDAT,STATUS='UNKNOWN',FORM='UNFORMATTED',
     1       BLOCKSIZE=1024)          !PUT CHANGE IN FILE
      WRITE (UNIT=4) J4,IB,LB,KB,NAN,LLBN,LLJZ3,LLLBN  !WRITE CHANGE
      CLOSE (4)
C
      OPEN (UNIT=4,NAME=IFLDAT,STATUS='UNKNOWN',FORM='UNFORMATTED',
     1       BLOCKSIZE=1024)     !TAKE CHANGED FILE AND RECALCULATE
C
C
C        PERFORM OPERATIONS ON FILE DATA AS WAS DONE TO
C                 INITIALLLY-ENTERED DATA BUT NOW USING CHANGED DATA
C
C
      READ (UNIT=4) J4,IB,LB,KB,NAN,LLBN,LLJZ3,LLLBN
      CLOSE (4)
      LZZ=0
      NAN=0
      JZ3=0
      LB(0)=LB(1)
      DO 8490 JZF=1,IB
      IF (LB(JZF).EQ.LB(JZF-1)) GOTO 8492
      NAN=NAN+1
      LLBN(NAN)=LZZ
      LLJZ3(NAN)=JZ3
      LLLBN(NAN)=LB(JZF-1)
      IF (JZF.EQ.IB) GOTO 8490   !END RECALCULATION OF FILE DATA
      LZZ=1
      IF (KB(JZF).NE.1) GOTO 8495
      JZ3=1
      GOTO 8490
 8495 JZ3=0
      GOTO 8490
 8492 IF (KB(JZF).NE.1) GOTO 8493
      JZ3=JZ3+1
 8493 LZZ=LZZ+1
 8490 CONTINUE
C
C       PUT RECALCULATED LLBN,LLJZ3,LLLBN ARRAYS IN FILE
C
      OPEN (UNIT=4,NAME=IFLDAT,STATUS='UNKNOWN',FORM='UNFORMATTED',
     1       BLOCKSIZE=1024)
      WRITE (UNIT=4) J4,IB,LB,KB,NAN,LLBN,LLJZ3,LLLBN
      CLOSE (4)
      OPEN (UNIT=4,NAME=IFLDAT,STATUS='UNKNOWN',FORM='UNFORMATTED',
```

```
     1        BLOCKSIZE=1024)    !READ OUT NEW FILE
      READ (UNIT=4) J4,IB,LB,KB,NAN,LLBN,LLJZ3,LLLBN
      CLOSE (4)
      IF (NONO.EQ.0.OR.NONO.EQ.1) GOTO 3332
 3334 TYPE *,'-----------------------------------------'
      GOTO 464      !SKIP NEW FLAW DATA ENTRY
C
C
C           THE FOLLOWING ROUTINE ALLOWS THE USER TO ENTER
C           FLAW SIZE DATA OBTAINED ON METALLOGRAPH
C
  378 IB=0    !INITIALIZE TOTAL FLAW # COUNTER
      NAN=0   !INITIALIZE # OF SPECIFIC FLAW SIZES COUNTER
      LZZ=0   !INITIALIZE TOTAL FLAWS/SP. SIZE COUNTER
      JZ3=0   !INITIALIZE FLAWS FOUND/SP. SIZE FLAW COUNTER
  379 TYPE *,'    '
      TYPE *,'         ENTER FLAW DATA FROM METALLOGRAPH'
      TYPE *,'         AND SLAM/RADIOGRAPHY (I3,I1 FORMAT)'
      TYPE *,'                   ENTER:'
      TYPE *,'    1) FLAW SIZE FROM METALLOGRAPH IN ASC. OR DESC. ORDER'
      TYPE *,'    2) 1 - IF FLAW FOUND ON SLAM'
      TYPE *,'       2 - IF FLAW NOT FOUND ON SLAM'
      TYPE *,'(ENTER 0(ZERO) AFTER LAST FLAW IS ENTERED)'
      TYPE *,'    '
  400 READ (5,401) JB,JU
  401 FORMAT (I3,I1)
      LB(0)=LB(1)
      IB=IB+1       !IB=# OF FLAWS ENTERED
      LB(IB)=JB   !STORE FLAW SIZES IN ARRAY
      KB(IB)=JU   !STORE SLAM RESULT IN ARRAY
      IF (LB(IB).EQ.LB(IB-1)) GOTO 402
      GOTO 403
  402 IF (KB(IB).NE.1) GOTO 405
      JZ3=JZ3+1   !KEEP TRACK OF # OF FLAWS FOUND/FL. SIZE
  405 LZZ=LZZ+1      !KEEP TRACK OF # OF SAME FLAWS
      GOTO 400
  403 NAN=NAN+1
      LLBN(NAN)=LZZ    !# OF FLAWS OF PARTICULAR SIZE
      LLJZ3(NAN)=JZ3 !# OF FLAWS FOUND OF PARTIC. SIZE
      LLLBN(NAN)=LB(IB-1)    !PARTICULAR SIZE FLAW/TH. SENS.
      LZZ=1
      IF (KB(IB).NE.1) GOTO 406
      JZ3=1
      GOTO 407
  406 JZ3=0
  407 IF (JB.EQ.0) GOTO 454
      GOTO 400
C
C
  454 TYPE *,'       '
      TYPE *,'---------------------------------------------'
      TYPE *,'              ENTER:'
      TYPE *,' 0 - TO FIRST STORE DATA IN FILE AND THEN GROUP'
      TYPE *,' ANY OTHER # - PROCEED DIRECTLY TO DATA GROUPING'
      READ (5,458) LM5
  458 FORMAT (I1)
      TYPE *,'------------------------------------------------'
      IF (LM5.NE.0) GOTO 464      !DO NOT STORE DATA
C
C           THE FOLLOWING ROUTINE STORES FLAW SIZE DATA ON DISK
C           (FOR DETAILED DOCUMENTATION OF STORING AND RETRIEVING
```

```
C           DATA, SEE RBOX PROGRAM).
C
      TYPE *,'     '
      TYPE *,'  TYPE IN A 6-CHARACTER NAME OF DATA FILE YOU WISH'
      TYPE *,'  TO STORE; (IF YOU INPUT O[ZERO], STORAGE WILL BE'
      TYPE *,'   ABORTED AND PROGRAM WILL PROCEED W/ DATA GR.)'
      TYPE *,'     '
      ACCEPT 459,IFLDAT(11),IFLDAT(12),IFLDAT(13),IFLDAT(14),
     1IFLDAT(15),IFLDAT(16)
  459 FORMAT (6A1)
      TYPE *,'------------------------------------------------'
      IF (IFLDAT(11).EQ.'0') GOTO 464
      OPEN (UNIT=4,NAME=IFLDAT,STATUS='UNKNOWN',FORM='UNFORMATTED',
     1       BLOCKSIZE=1024)
C
C          STORE FLAW SIZE DATA ON DISK
C
      WRITE (UNIT=4) J4,IB,LB,KB,NAN,LLBN,LLJZ3,LLLBN
      CLOSE (4)
      TYPE *,'     '
      WRITE (5,437) IFLDAT
  437 FORMAT (5X,20A1,1X,'HAS BEEN STORED')
      TYPE *,'-------------------------------------------------------'
C
C

  464 IF (MMM.EQ.3.OR.L99.EQ.3) GOTO 6028     !# OF FLAWS PLOT
      IF (L99.EQ.0 .OR. L99.EQ.1) GOTO 219    !OVERLAPPING/EQUAL INT.
      GOTO 2005     !OPT. PROB. ROUTINE
 6028 IF (L32.EQ.0) GOTO 6048   !RADIOGRAPHY
C
C
C
C          FLAW FREQUENCY ROUTINE
C
C
      DO 6030 L57=1,NAN    !# OF FLAWS PLOT/SLAM DATA
      IF (LLBN(L57).LE.27) GOTO 6029
      LLBN(L57)=27
      IF (LLJZ3(L57).LE.27) GOTO 6029
      LLJZ3(L57)=27
 6029 CALL GRFVCS (1,100,50+LLLBN(L57)*2,50+LLBN(L57)*16,
     150+LLLBN(L57)*2,50)       !TOTAL FLAWS OF PARTIC. SZ.
      CALL GRFVCS (1,255,50+LLLBN(L57)*2,50+LLJZ3(L57)*16,
     150+LLLBN(L57)*2,50)      !FLAWS FOUND
 6030 CONTINUE
      GOTO 8020      !END PROGRAM
 6048 DO 6050 L57=1,NAN    !# OF FLAWS PLOT/RADIOGRAPHY DATA
      IF (LLBN(L57).LE.27) GOTO 6049
      LLBN(L57)=27
      IF (LLJZ3(L57).LE.27) GOTO 6049
      LLJZ3(L57)=27
 6049 CALL GRFVCS (1,100,50+NINT(LLLBN(L57)*.8),50+LLBN(L57)*16,
     150+NINT(LLLBN(L57)*.8),50)     !# OF FLAWS OF PARTIC. SZ.
      CALL GRFVCS (1,255,50+NINT(LLLBN(L57)*.8),50+LLJZ3(L57)*16,
     150+NINT(LLLBN(L57)*.8),50)    !# OF FLAWS FOUND
 6050 CONTINUE
      CALL GRSBFD
      GOTO 8020    !END PROGRAM
C
C
```

```
C           OPTIMIZED PROBABILITY METHOD FOR GROUPING DATA
C
 2005 TYPE *,'       '
      DO 71 MOP=1,300     !INITIALIZE ALL ARRAYS
      LLR(MOP)=0
      IIQ(MOP)=0
      IXQ(MOP)=0
      KKQ(MOP)=0
      KXQ(MOP)=0
      AR11(MOP)=0
   71 CONTINUE
      TYPE *,'                 ENTER:'
      TYPE *,'    0 - TO WRITE ALL CALC. PROB. TO TERMINAL'
      TYPE *,'    ANY OTHER # - TO OMIT WRITING CALC. PROB.'
      READ (5,2007) MOM
 2007 FORMAT (I1)
      TYPE *,'----------------------------------------'
      TYPE *,'            ENTER:'
      TYPE *,'         0 - PLOT FLAW SIZE RANGE BARS'
      TYPE *,'   ANY OTHER # - DO NOT PLOT FLAW SIZE RANGE BARS'
      READ (5,987) MAZE
  987 FORMAT (I1)
      TYPE *,'       '
      TYPE *,'       '
      TYPE *,'-----------------------------------------------------'
      TYPE *,'   ENTER THE # OF BOUNDARY FLAW SIZES TO BE USED:'
      READ (5,2010) IIX
 2010 FORMAT (I2)
      TYPE *,'-------------------------------------------------------'
      TYPE *,'              IMPORTANT!!'
      TYPE *,'   NOTE: PLEASE TYPE BOUNDARY FLAW SIZES IN'
      TYPE *,'                ASCENDING ORDER'
      TYPE *,'-------------------------------------------------------'
      DO 3050 JJX=1,IIX
      WRITE (5,4000) JJX
 4000 FORMAT (' BOUNDARY FLAW SIZE #',I3,'=(ENTER SIZE IN MICRONS)')
      READ (5,5555) LLX
 5555 FORMAT (I3)
      LLR(JJX)=LLX       !STORE BOUNDARY FLAW SIZES IN ARRAY
 3050 CONTINUE
      TYPE *,'            '
      TYPE *,'-----------------------------------------------------'
C
C           THIS ROUTINE PLACES FLAWS IN PROPER INTERVALS
C
C
      IIQ(1)=0      !INITIALIZE # OF FLAWS/INTERVAL COUNTER
      IXQ(1)=0      !SAME AS ABOVE FOR IXQ
      KKQ(1)=0      !INITIALIZE # OF FLAWS FOUND/INTERVAL COUNTER
      KXQ(1)=0      !SAME AS ABOVE FOR KXQ
      JJQ=1        !SET  INTERVAL COUNTER INITIALLY TO 1
 3057 DO 5900 NNB=1,IB         !FOR EACH FLAW
      IF (LB(NNB).GE.LLR(JJQ).AND.LB(NNB).LE.LLR(JJQ+1)) GOTO 5050
      GOTO 5900
 5050 IIQ(JJQ)=IIQ(JJQ)+1     !KEEP TRACK OF # OF FLAWS/INTERVAL
      IXQ(JJQ)=IXQ(JJQ)+1     !SAME AS ABOVE FOR IXQ ARRAY
      IF (KB(NNB).EQ.2) GOTO 5900      !FLAW NOT SEEN ON SLAM
      KKQ(JJQ)=KKQ(JJQ)+1     !KEEP TRACK OF # OF FLAWS SEEN/INTERVAL
      KXQ(JJQ)=KXQ(JJQ)+1      !SAME AS ABOVE FOR KXQ ARRAY
 5900 CONTINUE
      WRITE (5,5910) KKQ(JJQ),IIQ(JJQ),LLR(JJQ),LLR(JJQ+1)
```

```
 5910 FORMAT (1X,I3,1X,'OUT OF',I3,1X,'FLAWS BETWEEN',1X,I4,1X
     1,'AND',I4,1X,'MICRONS WERE FOUND ON SLAM')
      TYPE *,'      '
      JJQ=JJQ+1        !INCREMENT INTERVAL COUNTER
      IF (JJQ.EQ.IIX) GOTO 6001      !PROCEED TO PROB. CALCS.
      GOTO 3057        !TRY ALL FLAWS AGAIN W/NEW INTERVAL
C
C          THIS ROUTINE CALCULATES PROBABILITIES (OPT. PROB.)
C
C
 6001 MMQ=IIX-1       !SET MMQ COUNTER INITIALLY TO # OF INTERVALS
C
 6100 JJQ=MMQ         !SET JJQ TO MMQ
      DO 6200 LED=1,IIX-1         !FOR EACH INTERVAL
      IIQ(LED)=IXQ(LED) !RESET IIQ VALUE FOR CORRECT CUM. PROB. CALC.
      KKQ(LED)=KXQ(LED) !RESET KKQ VALUE FOR CORRECT CUM. PROB. CALC.
 6200 CONTINUE
C
 6500 AR1=FLOATI(IIQ(JJQ))    !CHANGE IIQ TO REAL
      AR2=FLOATI(KKQ(JJQ))    !CHANGE KKQ TO REAL
      AR3=FLOATI(IAR3)/100.     !CHANGE CONF. LEVEL TO REAL/DECIMAL
      CALL BIN(AR1,AR2,AR3,AR10)     !SUBROUTINE FOR PROB. CALC.
      AR11(JJQ)=AR10
      IF (MOM.NE.0) GOTO 6502
      WRITE (5,6501) JJQ,AR11(JJQ)
 6501 FORMAT (10X,'CALC. PROB.(',I2,')='F5.3)
 6502 IF (JJQ.EQ.1) GOTO 7000     !FINISHED W/THIS INTERVAL
      JJQ=JJQ-1          !DECREMENT JJQ BY 1
      IIQ(JJQ)=IIQ(JJQ+1)+IIQ(JJQ)     !CUMULATIVE TOTAL FLAWS
      KKQ(JJQ)=KKQ(JJQ+1)+KKQ(JJQ)     !CUMULATIVE FLAWS FOUND
      GOTO 6500
C
C
C         ROUTINE TO GET MAX PROBABILITY FROM ABOVE CALC. PROBABILITIES
C
 7000 PMAX=0.
      DO 7020 JKQX=1,MMQ      !FOR EACH PROBABILITY
      IF (AR11(JKQX).GT.PMAX) GOTO 7010       !TEST
      GOTO 7020
 7010 PMAX=AR11(JKQX)
      JKQ=JKQX
 7020 CONTINUE
C
 5920 WRITE (5,5930) IAR3,PMAX
 5930 FORMAT (1X,'AT',1X,I2,'%',1X,'CONFIDENCE, THE LOWER-BOUND
     1 PROBABILITY OF DETECTION=',1X,F5.3)
      WRITE (5,5940) (LLR(MMQ)+(LLR(MMQ+1)-LLR(MMQ)))
 5940 FORMAT (20X,'AT FLAW SIZE=',1X,I3)
      LLMX=LLMX+1        !KEEP TRACK OF # OF PTS. TO BE PLOTTED
      TYPE *,'    '
      IF (L32.EQ.0) GOTO 5943   !PLOT FOR RADIOGR.
      XYDATA(2*LLMX-1)=50+(LLR(MMQ)+(LLR(MMQ+1)-LLR(MMQ)))*2   !FL.SZ. C.
      XYDAT(2*LLMX-1)=50+(LLR(MMQ)+(LLR(MMQ+1)-LLR(MMQ)))*2 !TH.PL.
      GOTO 5944          !SKIP RAD. POINTS
 5943 XYDATA(2*LLMX-1)=50+NINT((LLR(MMQ)+(LLR(MMQ+1)-LLR(MMQ)))*.8) !RD.
      XYDAT(2*LLMX-1)=50+NINT((LLR(MMQ)+(LLR(MMQ+1)-LLR(MMQ)))*.8) !RD.
 5944 XYDATA(2*LLMX)=50+(NINT(PMAX*100.)*4.)    !P.O.D. COOR.
      XYDAT(2*LLMX)=49+(NINT(PMAX*100.)*4.)     !THICKEN PLOT
C
C           PLOT POINTS USING ABOVE COORDINATES (VISIBILITY AID)
C
```

```
      CALL GRFAR (1,254,0,0,XYDATA(2*LLMX-1)-2,XYDATA(2*LLMX)-2,4,4)
C
      IF (MAZE.NE.0) GOTO  5947  !DO NOT PLOT FL. SZ. RANGE BARS
C
C              PLOT FLAW SIZE RANGE BARS
C
      IF (L32.EQ.0) GOTO 5946  !PLOT FOR RADIOGR.
      IF (JKQ.EQ.1.AND.MMQ.EQ.1) GOTO 4695
      MKQ=MMQ+1
      GOTO 4696
 4695 MKQ=MMQ+1
 4696 CALL GRFVC (1,150,0,0,XYDATA(2*LLMX-1)-(LLR(MKQ)-
     1LLR(JKQ))*2,XYDATA(2*LLMX),XYDATA(2*LLMX-1),XYDATA(2*LLMX))
C
      CALL GRFVC (1,150,0,0,XYDATA(2*LLMX-1)-(LLR(MKQ)-
     1LLR(JKQ))*2,XYDATA(2*LLMX)-2,XYDATA(2*LLMX-1)-
     1(LLR(MKQ)-LLR(JKQ))*2,XYDATA(2*LLMX)+2)
      GOTO 5947        !SKIP RADIOGRAPHIC POINTS
C
 5946 IF (JKQ.EQ.1.AND.MMQ.EQ.1) GOTO 4211
      MKQ=MMQ+1
      GOTO 4213
 4211 MKQ=MMQ+1
 4213 CALL GRFVC (1,150,0,0,XYDATA(2*LLMX-1)-NINT((LLR(MKQ)
     1-LLR(JKQ))*.8),XYDATA(2*LLMX),XYDATA(2*LLMX-1),
     1XYDATA(2*LLMX))
C
      CALL GRFVC (1,150,0,0,XYDATA(2*LLMX-1)-NINT((LLR(MKQ)
     1-LLR(JKQ))*.8),XYDATA(2*LLMX)-2,
     1XYDATA(2*LLMX-1)-NINT((LLR(MKQ)-LLR(JKQ))*.8),
     1XYDATA(2*LLMX)+2)
C
C
C
 5947 WRITE (5,5949) MKQ,JKQ,LLR(JKQ),LLR(MKQ)
 5949 FORMAT (10X,I3,5X,I3,5X,I3,5X,I3)
      MMQ=MMQ-1
      IF (MMQ.EQ.0) GOTO 8010
      GOTO 6100
 8010 CALL GRFVL (1,254,0,0,XYDATA,LLMX)  !PLOT OF P.O.D. VS. FLAW SIZE
      CALL GRFVL(1,254,0,0,XYDAT,LLMX)  !THICKEN PLOT LINE
      CALL GRSBFD
      LLMX=0
      N99=1000
      TYPE *,'              ENTER:'
      TYPE *,'   0 - TO GROUP DATA USING EQUAL/OVERL. INT. METHOD'
      TYPE *,'   1 - TO USE DIFFERENT CONFIDENCE LEVEL'
      TYPE *,'   2 - TO USE DIFFERENT INTERVALS'
      TYPE *,'   3 - TO PLOT # OF FLAWS VS. FL.SZ./TH. SENS.'
      TYPE *,'   4 - TO END PROGRAM'
      READ (5,8011) MMM
 8011 FORMAT (I1)
      TYPE *,'-----------------------------------------------'
      IF (MMM.EQ.0) GOTO 611
      IF (MMM.EQ.1) GOTO 629
      IF (MMM.EQ.2) GOTO 2178
      IF (MMM.EQ.3) GOTO 2178
      GOTO 8020
C
C
C          END OF OPTIMIZED PROBABILITY METHOD
```

```
C
C          START OF EQUAL/OVERLAPPING INTERVAL METHOD FOR DATA
C
  219 TYPE *,'     '
      TYPE *,'     '
      DO 70 MB=1,100     !INITIALIZE ALL ARRAYS
      LR(MB)=0
   70 CONTINUE
      DO 60 MB=1,200
      JR(MB)=0
   60 CONTINUE
      TYPE *,'     '
      TYPE *,'     ENTER THE # OF BOUNDARY FLAW SIZES TO BE USED!'
      TYPE *,'  (REMEMBER! BOUNDARY FLAW SIZES MUST BE EQUALLY SPACED)'
      TYPE *,'             (EX. 40,80,120,160 MICRONS)'
      READ (5,210) IX
  210 FORMAT (I2)
      TYPE *,'-----------------------------------------------------------'
      DO 305 JX=1,IX
      WRITE (5,40) JX
   40 FORMAT ('     BOUNDARY FLAW SIZE  #',I3,'=(ENTER SIZE IN MICRONS)')
      READ (5,55) LX
   55 FORMAT (I3)
      LR(JX)=LX
  305 CONTINUE
      TYPE *,'     '
      TYPE *,'  ENTER THE AMOUNT OF OVERLAP (%) DESIRED'
      READ (5,20) N
   20 FORMAT (I3)
      TYPE *,'--------------------------------------------------'
      Z=0
C
C          CALCULATE OVERLAP FLAW SIZE BOUNDARIES BASED ON
C          # OF ORIGINAL BAOUNDARY FLAW SIZES ENTERED, THE
C          ORIGINAL SIZES THEMSELVES, AND THE AMOUNT OF OVERLAP
C
      IEO=IIFIX((FLOATI(LR(2))-FLOATI(LR(1)))*FLOATI(100-N)/100.)
      IF (IEO.NE.0) GOTO 838
      IEO=1
  838 DO 100 Y=1,IX-1
      DO 200 X=LR(Y),LR(Y+1),IEO
      IF (X.EQ.LR(1)) GOTO 199   !DON'T SKIP FIRST BOUNDARY
      IF (X.EQ.LR(Y)) GOTO 200      !DON'T REPEAT BOUNDARIES
  199 Z=Z+1     !KEEP TRACK OF HOW MANY BOUNDARY FLAW SIZES
      JR(Z)=X   !STORE CALCULATED BOUNDARIES IN ARRAY
  200 CONTINUE
  100 CONTINUE
      DO 300 MO=1,Z   !WRITE OVERLAP BOUNDARIES TO TERMINAL
      WRITE (5,301) MO,JR(MO)
  301 FORMAT ('  FLAW SIZE #',I3,'=',1X,I3)
  300 CONTINUE
      TYPE *,'     '
C
C
C
C
C
C
C          THIS ROUTINE PLACES FLAWS IN PROPER INTERVALS
C
```

```
C
  500 IQ=0      !INITIALIZE # OF FLAWS/INTERVAL COUNTER
      KQ=0      !INITIALIZE # OF FLAWS FOUND/INTERVAL COUNTER
      DO 550 JQ=1,Z          !FOR EACH CALCULATED INTERVAL
      IF (JR(JQ).GT.(JR(Z)-(LR(2)-LR(1)))) GOTO 550
      DO 590 NB=1,IB         !FOR EACH FLAW
      IF (LB(NB).GE.JR(JQ).AND.LB(NB).LE.JR(JQ)+(LR(2)-LR(1)))
     1 GOTO 505
      GOTO 590
  505 IQ=IQ+1         !KEEP TRACK OF # OF FLAWS/INTERVAL
      IF (KB(NB).EQ.2) GOTO 590  !FLAW NOT SEEN ON SLAM
      KQ=KQ+1         !KEEP TRACK OF # OF FLAWS SEEN ON SLAM/INTERVAL
  590 CONTINUE
      WRITE (5,591) KQ,IQ,JR(JQ),JR(JQ)+(LR(2)-LR(1))
  591 FORMAT (1X,I3,1X,'OUT OF',I3,1X,'FLAWS BETWEEN',1X,I4,1X,'AND',
     1I4,1X,'MICRONS WERE FOUND ON SLAM')
      TYPE *,'     '
C
C
      AR1=FLOATI(IQ)      !CHANGE IQ TO REAL
      AR2=FLOATI(KQ)      !CHANGE KQ TO REAL
      AR3=FLOATI(IAR3)/100.
C
C
      CALL BIN(AR1,AR2,AR3,AR10)      !SUBROUTINE FOR PROB. CALC.
C
C
C
C


  592 WRITE (5,593) IAR3,AR10
  593 FORMAT (1X,'AT',1X,I2,'%',1X,'CONFIDENCE, THE LOWER-BOUND
     1 PROBABILITY OF DETECTION=',1X,F4.2)
      LMX=LMX+1     !KEEP TRACK OF # OF POINTS TO BE PLOTTED
      TYPE *,'     '
      IF (L32.EQ.0) GOTO 594        !RADIO. PTS.
      XYDATA(2*JQ-1)=50+(JR(JQ)+(LR(2)-LR(1)))*2  !FLAW SIZE PIXEL COOR.
      XYDAT(2*JQ-1)=50+(JR(JQ)+(LR(2)-LR(1)))*2  !THICKEN PLOT LINE
      GOTO 595    !SKIP RADIO. PTS.
  594 XYDATA(2*JQ-1)=50+NINT((  (JQ)+(LR(2)-LR(1)))*.8)     !RADIO.
      XYDAT(2*JQ-1)=50+NINT((JR(JQ)+(LR(2)-LR(1)))*.8)    !RADIO.
  595 XYDATA(2*JQ)=50+IIFIX(AR10*100.*4.)       ! P.O.D. PIXEL COOR.
      XYDAT(2*JQ)=49+IIFIX(AR10*100.*4.)        !THICKEN PLOT LINE
C
C          PLOT POINTS USING ABOVE COORDINATES (VISIBILITY AID)
C
      CALL GRFAR (1,255,0,0,XYDATA(2*JQ-1)-2,XYDATA(2*JQ)-2,4,4)
C
C       PLOT FLAW SIZE RANGE BARS
C
C
      IF (L32.EQ.0) GOTO 596      !RADIO. PTS.
      CALL GRFVC (1,150,0,0,XYDATA(2*JQ-1)-(LR(2)-LR(1))*2,
     1XYDATA(2*JQ),XYDATA(2*JQ-1),XYDATA(2*JQ))
C
      CALL GRFVC (1,150,0,0,XYDATA(2*JQ-1)-(LR(2)-LR(1))*2,
     1XYDATA(2*JQ)-2,XYDATA(2*JQ-1)-(LR(2)-LR(1))*2,
     1XYDATA(2*JQ)+2)
      GOTO 597     !SKIP RADIO. PTS.
  596 CALL GRFVC (1,150,0,0,XYDATA(2*JQ-1)-NINT((LR(2)-LR(1))*.8),
     1XYDATA(2*JQ),XYDATA(2*JQ-1),XYDATA(2*JQ))
```

```
C
      CALL GRFVC (1,150,0,0,XYDATA(2*JQ-1)-NINT((LR(2)-LR(1))*.8),
     1XYDATA(2*JQ)-2,XYDATA(2*JQ-1)-NINT((LR(2)-LR(1))*.8),
     1XYDATA(2*JQ)+2)
C
  597 IQ=0         !RESET FLAW COUNTER FOR NEXT INTERVAL
      KQ=0         !RESET FLAWS FOUND COUNTER FOR NEXT INTERVAL
  550 CONTINUE
      CALL GRFVL (1,255,0,0,XYDATA,LMX) !PLOT OF P.O.D. VS. FLAW SIZE
      CALL GRFVL (1,255,0,0,XYDAT,LMX)  !THICKEN PLOT LINE W/XYDAT PTS.
      CALL GRSBFD
      LMX=0
      N99=1000
      TYPE *,'            ENTER:'
      TYPE *,'  0 - TO GROUP DATA USING ANOTHER METHOD'
      TYPE *,'  1 - TO USE DIFFERENT CONFIDENCE LEVEL'
      TYPE *,'  2 - TO USE DIFFERENT INTERVALS'
      TYPE *,'  3 - TO PLOT # OF FLAWS VS. FL.SZ./TH. SENS.'
      TYPE *,'  4 - TO END PROGRAM'
      READ (5,542) MMM
  542 FORMAT (I1)
      TYPE *,'------------------------------------------------'
      IF (MMM.EQ.0) GOTO 611
      IF (MMM.EQ.1) GOTO 629
      IF (MMM.EQ.2) GOTO 2178
      IF (MMM.EQ.3) GOTO 2178
 8020 CALL GRSBFD
      CALL GRSEND
      END
>
```

```
C           THE FOLLOWING SUBROUTINE CALCULATES THE PROBABILITY OF
C           DETECTION OF FLAWS ON THE SLAM (OR OTHER NDE INSTRUMENT),(AR10),
C           GIVEN THE SIZE RANGE, CONFIDENCE LEVEL (AR3), TOTAL # OF
C           FLAWS (AR1), AND THE # OF FLAWS FOUND (AR2).
C
      SUBROUTINE BIN(AR1,AR2,AR3,AR10)
    1 IF(AR2)2,2,4
    2 AR10=0.0
    3 RETURN
    4 IF(AR2-AR1)7,5,5
    5 AR10=(1.0-AR3)**(1.0/AR1)
    6 RETURN
    7 ATT=2.0*AR2
    8 IF(ATT-AR1)9,9,12
    9 AR4=AR2-1.0
   10 AR5=-1.0
   11 GO TO 15
   12 AR4=AR1-AR2
   13 AR3=1.0-AR3
   14 AR5=-1.0
   15 AR10=0.5
   16 AR6=1.0
   17 AR8=0.0
   18 AR9=1.0
   19 AR11=AR1
   20 AR7=(AR10**AR8)*((1.0-AR10)**(AR1-AR8))
   21 IF(AR8-AR4)22,27,22
   22 AR8=AR8+1.0
   23 AR9=AR9*AR11/AR8
   97 IF (AR9.GT.10.**30.) GOTO 98
   24 AR11=AR11-1.0
   96 GOTO 25
   98 AR9=10.**30.
   99 GOTO 24
   25 AR7=AR7+AR9*(AR10**AR8)*((1.0-AR10)**(AR1-AR8))
   26 GO TO 21
   27 IF(AR3-AR7)28,28,30
   28 AR20=AR10-AR5/(2.0**(AR6+1.0))
   29 GO TO 31
   30 AR20=AR10+AR5/(2.0**(AR6+1.0))
   31 CCC=ABS(AR7-AR3)
   32 IF(CCC-0.0001)36,36,33
   33 AR6=AR6+1.0
   34 AR10=AR20
   35 GO TO 17
   36 IF(ATT-AR1)6,6,37
   37 AR10=1.0-AR10
   38 RETURN
   39 END
```

APPENDIX C

SEEDED SURFACE VOID INSPECTION DATA

Figures 13 to 20, generated using the Fortran program described in appendix B, show the raw data obtained from the SLAM inspections of the seeded test specimens. Each figure shows the void size distribution plot, that is, the number and size of voids detected and examined for each particular material, specimen thickness, and surface condition. The curves of probability of detection (at ≥ 0.95 confidence level) as a function of void diameter (POD) in figures 8 to 10 were derived from these data.

REFERENCES

1. Shulz, R.B., "Overview of U.S. Department of Energy Ceramic Gas Turbine Program," Ceramics for High-Performance Applications III: Reliability, 1983, pp. 21-28, Plenum Press, New York.

2. Katz, R.N., "Ceramics for Vehicular Engines: State-of-the-Art?," Energy and Ceramics, 1980, pp. 449-467, Elsevier, Amsterdam.

3. Harper, J.E., "ARPA/NAVAIR Ceramic Gas Turbine Engine Demonstration Program," Ceramics for High-Performance Applications III: Reliability, 1983, pp. 645-664, Plenum Press, New York.

4. Lenoe, E.M., "Recent Accomplishments and Research Needs in Structural Ceramics," Ceramics for High-Performance Applications III: Reliability, 1983, pp. 3-18, Plenum Press, New York.

5. Bortz, S., "Reliability of Ceramics for Heat Engine Applications," Ceramics for High-Performance Applications III: Reliability, 1983, pp. 445-473, Plenum Press, New York.

6. Evans, A.G., G.S. Kino, B.T. Khuri-Yakub, B.R. Jittman, "Failure Prediction in Structural Ceramics," Materials Evaluation, Vol. 35, Apr. 1977, pp. 85-96.

7. Klima, S.J., "NDE for Heat Engine Ceramics," NASA TM-86949, 1984.

8. Rice, R.W., J.J. Mecholsky, S.W. Freiman, and S.M. Morey, "Failure Causing Defects in Ceramics: What NDE Should Find," NRL-MR-4075, Naval Research Lab, 1979.

9. Kupperman, D.S., L. Pahis, D. Yuhas, and T.E. McGraw, "Acoustic Microscopy Techniques for Structural Ceramics," American Ceramic Society Bulletin, Vol. 59, Aug. 1980, pp. 814-816.

10. Heitman, P.W., and P.K. Khandelwal, "Development and Characterization of Ceramic Turbine Components," Ceramics for High-Performance Applications III: Reliability, 1983, pp. 645-664, Plenum Press, New York.

11. Bowen, H.K., "Basic Research Needs on High Temperature Ceramics for Energy Applications." Materials Science and Engineering, Vol. 44, June 1980, pp. 1-56.

12. Evans, A.G., "Structural Reliability: A Processing-Dependent Phenomenon," Journal of the American Ceramic Society, Vol. 65, Mar. 1982, pp. 127-137.

13. Rice, R.W., and D. Lewis III, "Limitations and Challenges in Applying Fracture Mechanics to Ceramics," Fracture Mechanics of Ceramics, Vol. 5, 1983, pp. 659-676, Plenum Press, New York.

14. McCauley, J.W., "The Role of Characterization in Emerging High Performance Ceramic Materials," American Ceramic Society Bulletin, Vol. 63, Feb. 1984, pp. 263-265.

15. Yuhas, D.E., and L.W. Kessler, "Defect Characterization by Means of The Scanning Laser Acoustic Microscope (SLAM)," Acoustical Imaging, Vol. 9, 1980, pp. 301-303, Plenum Press, New York.

16. Yuhas, D.E., T.E. McGraw, and L.W. Kessler, "Scanning Laser Acoustic Microscope Visualization of Solid Inclusions in Silicon Nitride," Proceedings of the DARPA/AFML Review of Progress in Quantitative Nondestructive Evaluation, 1980, pp. 683-690, (AFWAL-TR-80-4078, AD-A094826).

17. Packman, P.F., "Reliability of Flaw Detection by Nondestructive Inspection," Metals Handbook, Vol. 11, Nondestructive Inspection and Quality Control, 1976, pp. 414-424, American Society For Metals, Metals Park, OH.

18. Berens, A.P., and P.W. Hovey, "Flaw Detection Reliability Criteria," AFWAL-TR-84-4022, vol. I, Air Force Wright Aeronautical Lab, 1984, (AD-A142001).

19. Dowdy, S., and S. Wearden, "Binomial Distributions," Statistics For Research, 1983, Chapter 3, Wiley, New York.

20. Yee, B.G.W., F.H. Chang, J.C. Couchman, G.H. Lemon, and P.F. Packman, "Assessment of NDE Reliability Data," NASA-CR-134991, 1976, General Dynamics, Fort Worth, TX.

TABLE I. SPECIMEN CHARACTERIZATION AND VOID DETECTABILITY DATA

Test bar material	Typical peak-to-valley surface roughness, μm		Average bulk density		Average dimensions (length by width), mm	Thickness, mm	Diameter range of seeded voids, μm		$\frac{\text{Voids detected}}{\text{Voids examined}}$ using SLAM			
									As-fired specimens		Hand-polished specimens	
	As-fired specimens	Hand-polished specimens	g/cm^3	Percent theoretical			As-fired specimens	Hand-polished specimens	Ratio	Percentage	Ratio	Percentage
Sintered silicon nitride, Si_3N_4	4 to 11	0.5 to 1.5	3.230	100	30 by 6	[a]2.1 to 2.2 (2)	40 to 120	60 to 140	39/45	45	48/48	97
						[a]2.9 to 3.2 (3)	45 to 130	60 to 165	29/40		37/37	
						[a]3.8 to 4.1 (4)	50 to 130	55 to 150	61/199		177/185	
Sintered silicon carbide, SiC	3 to 9	0.5 to 1.5	3.126	97	30 by 6	[a]2.8 to 3.0 (3)	50 to 160	NA[b]	140/155	88	NA[b]	NA[b]
						[a]3.7 to 4.0 (4)	50 to 165	NA[b]	166/191		NA[b]	

[a]The number in parentheses indicates approximate thickness of specimens.
[b]The notation "NA" means statistical data not available.

TABLE II. - SAMPLE SET OF DATA

Interval	Diameter range, μm	Measured diameter of voids seeded, μm	Was void detected?	$\frac{\text{Voids detected}}{\text{Voids examined}}$
A	110 to 120	116	Yes	4/4
		116	Yes	
		112	Yes	
		112	Yes	
B	100 to 110	106	Yes	6/6
		106	Yes	
		104	Yes	
		104	Yes	
		100	Yes	
		100	Yes	
C	90 to 99	98	Yes	8/12
		98	Yes	
		98	Yes	
		98	No	
		96	Yes	
		96	Yes	
		96	Yes	
		93	Yes	
		93	No	
		91	Yes	
		91	No	
		91	No	

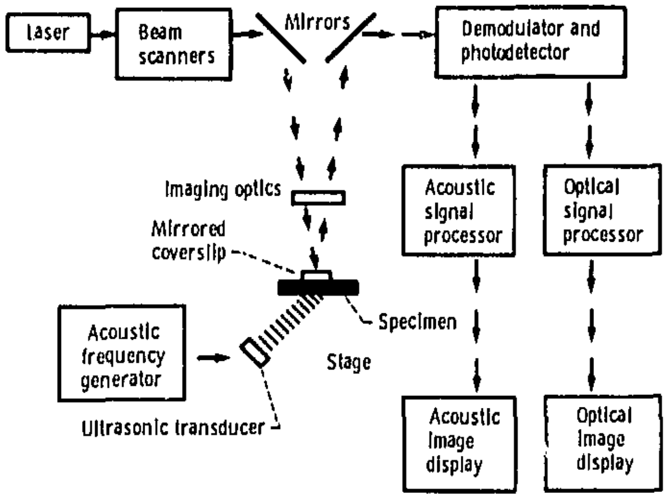

(a) Schematic diagram of scanning laser acoustic microscope.

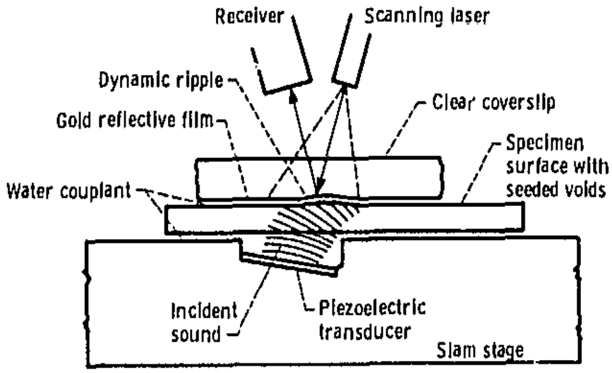

(b) Acoustic microscopy technique for ceramic bars.

Figure [illegible]. - Scanning laser acoustic microscope.

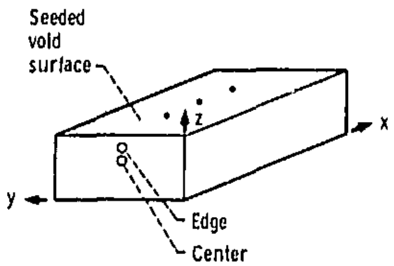

(a) Schematic of specimen showing center and edge areas where micrographs were obtained.

Figure 2. - Center and edge optical micrographs of polished, unetched ceramic test specimen cross sections showing porosity within material.

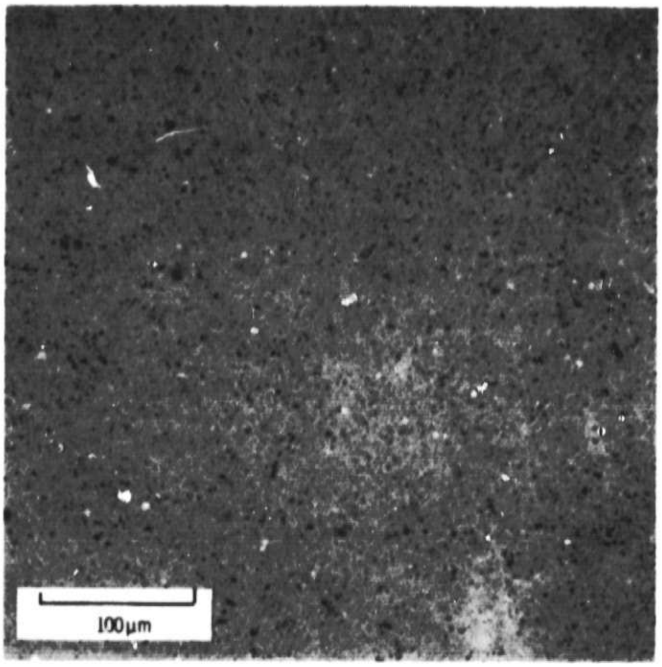

(b) Sintered silicon nitride (center).

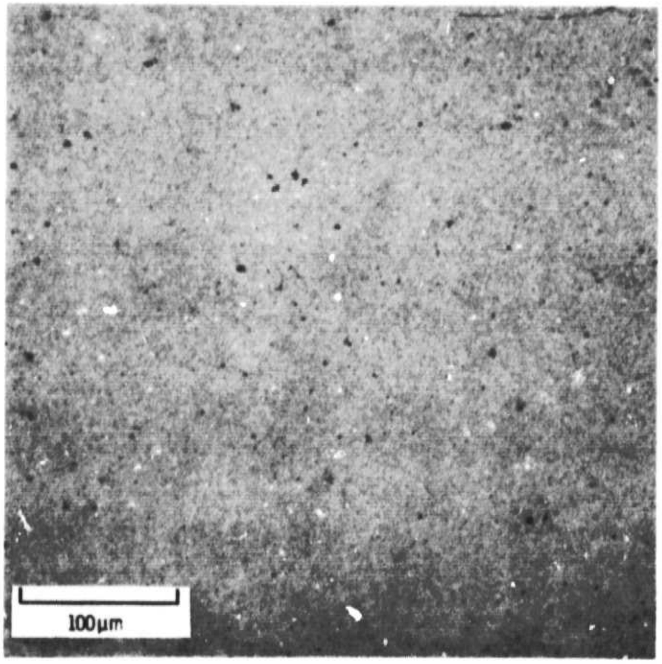

(c) Sintered silicon nitride (edge).

Figure 2. - Continued.

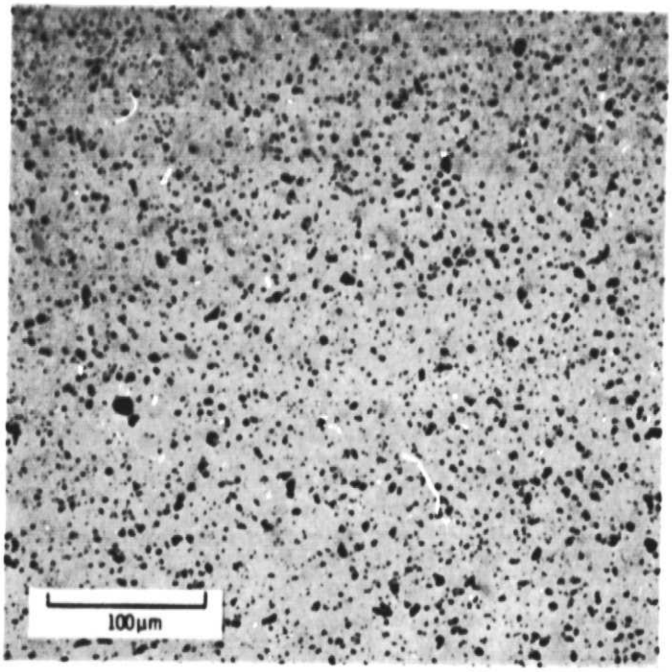

(d) Sintered silicon carbide (center).

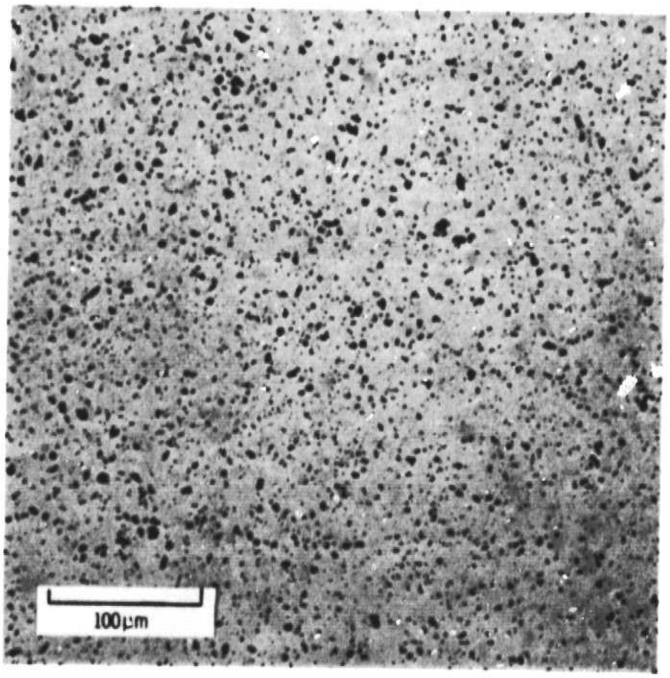

(e) Sintered silicon carbide (edge).

Figure 2. - Concluded.

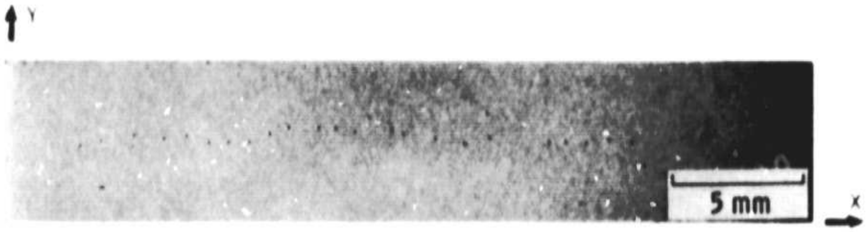

Figure 3. - Optical photograph of as-fired silicon nitride test specimen surface showing location of seeded surface voids along longitudinal (x) axis.

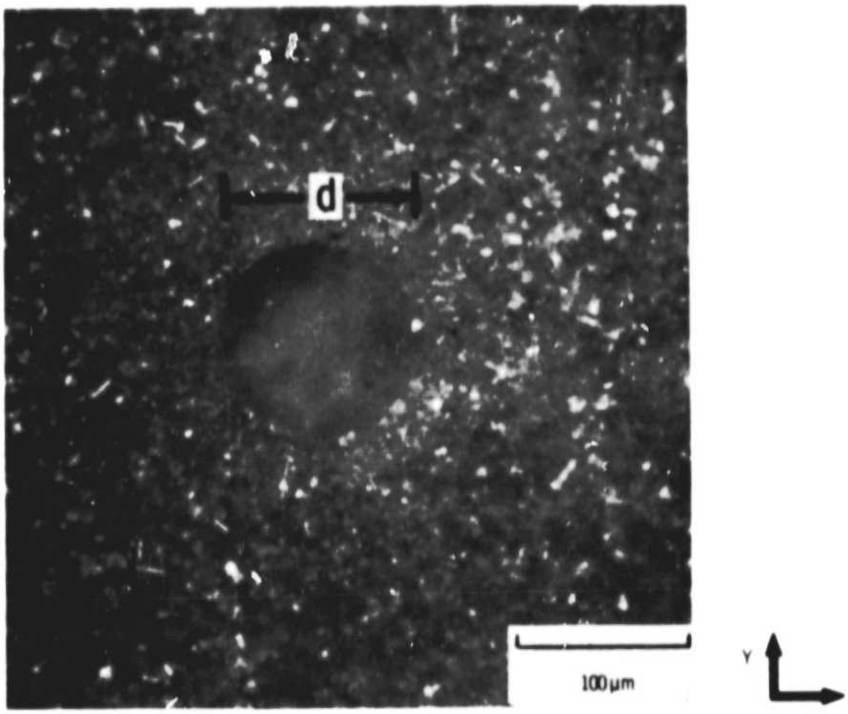

(a) As-fired specimen.

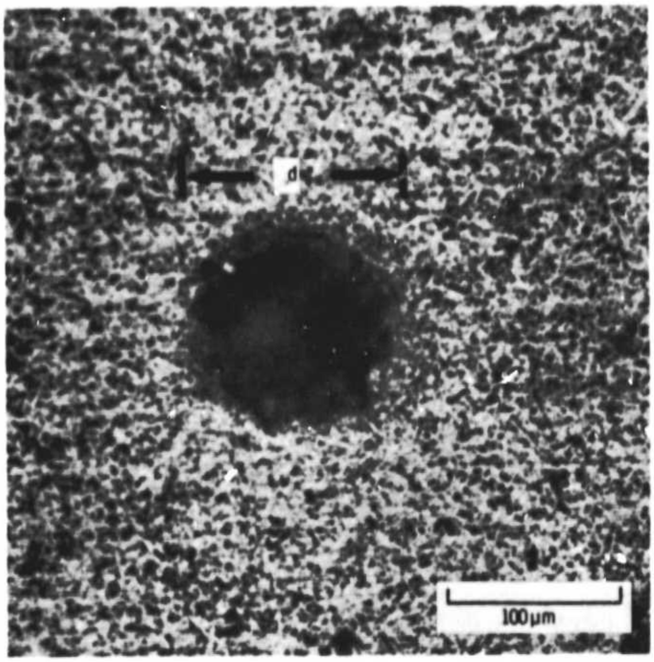

(b) Polished specimen.

Figure 4. - Optical micrographs of seeded surface void in sintered silicon nitride test specimen in as-fired condition and after polishing. Note change in diameter of void after polishing.

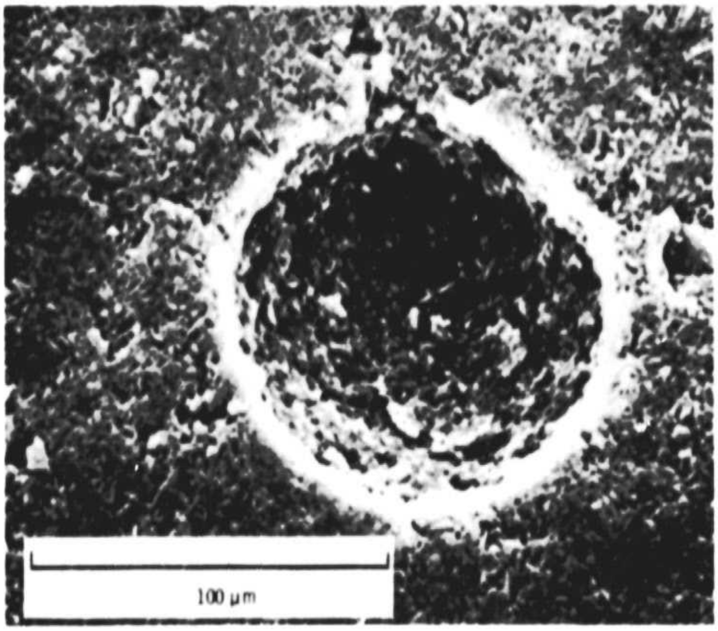

(a) Electron micrograph of void in as-fired specimen.

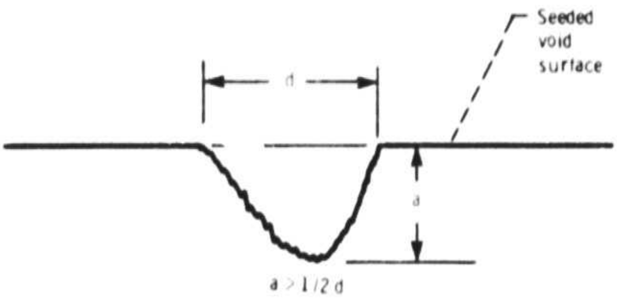

(b) Schematic of void in as-fired sintered silicon nitride.

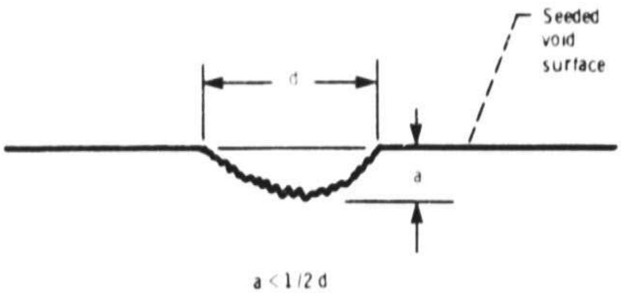

(c) Schematic of void in as-fired sintered silicon carbide.

Figure 5. - Electron micrograph of a typical seeded surface void and side-view diagrams of voids.

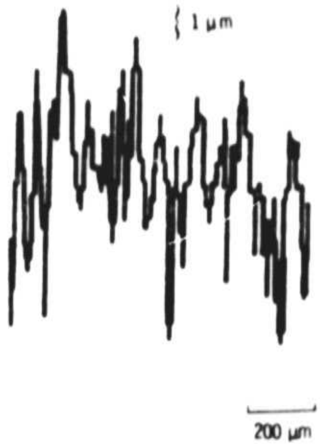

(a) As-fired surface profile.

(b) Acoustic micrograph of as-fired specimen.

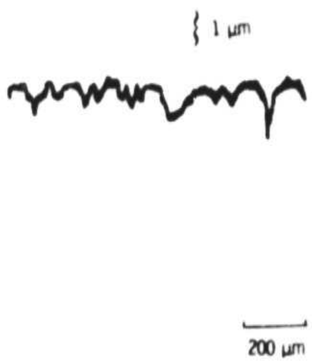

(c) Hand-polished surface profile.

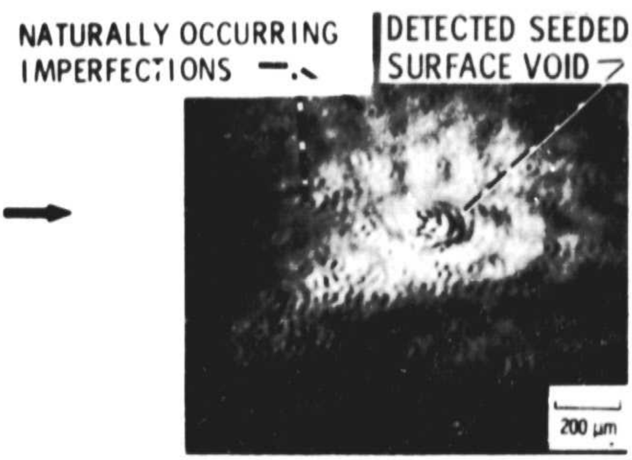

(d) Acoustic micrograph of hand-polished specimen.

Figure 6. - Representative surface profiles and corresponding scanning laser acoustic micrographs for sintered silicon nitride specimens.

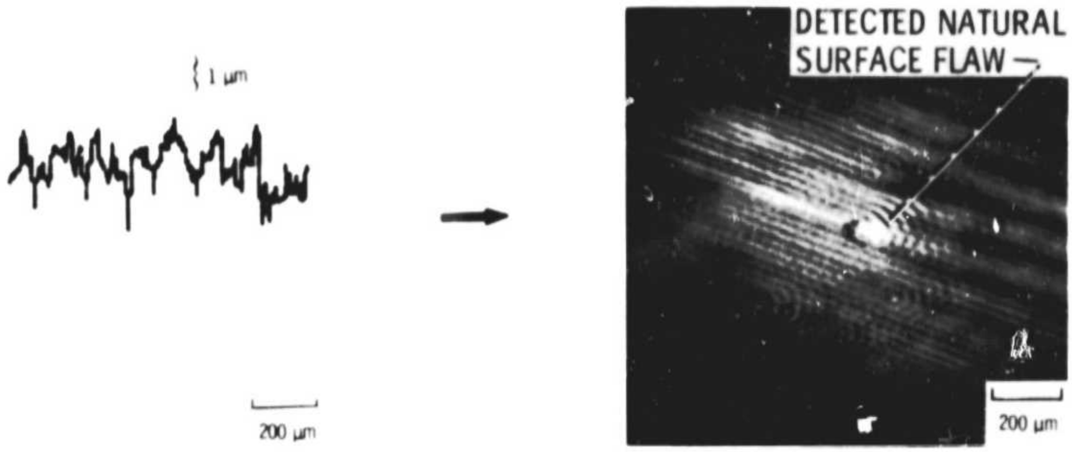

(e) Diamond - ground surface profile taken perpendicular to grinding marks.

(f) Acoustic micrograph of diamond - ground specimen.

Figure 6. - Concluded.

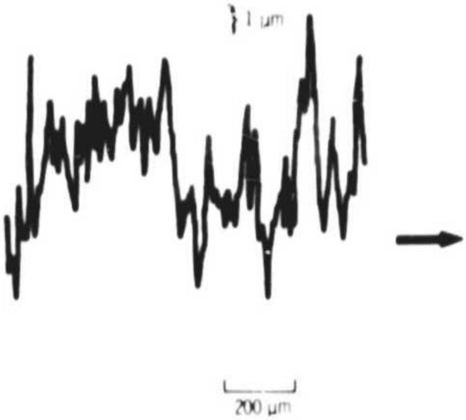

(a) As-fired surface profile.

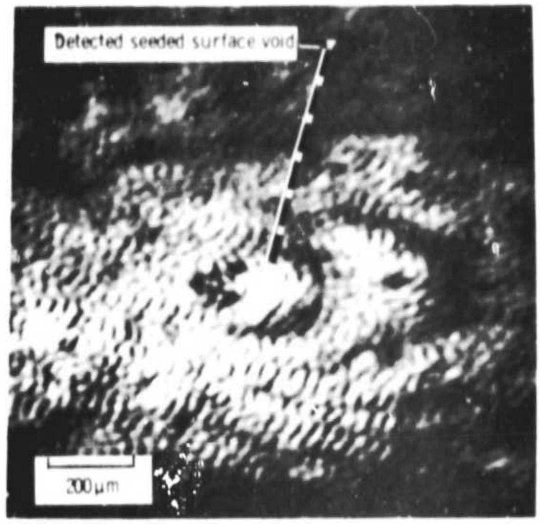

(b) Acoustic micrograph of as-fired specimen.

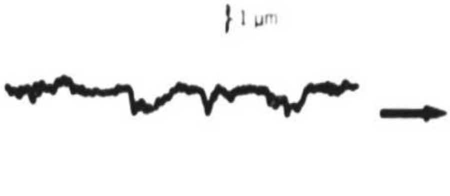

(c) Hand-polished surface profile.

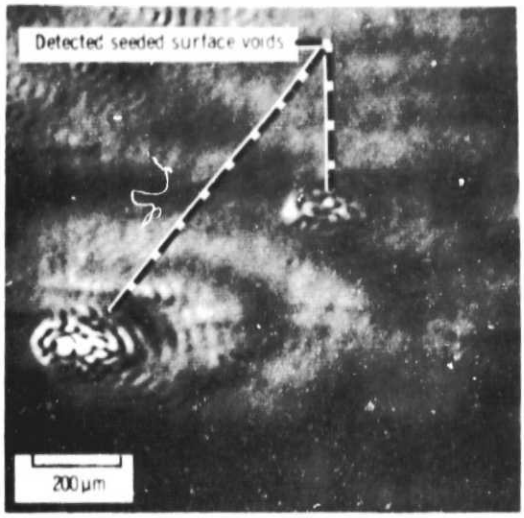

(d) Acoustic micrograph of hand-polished specimen.

Figure 7. - Representative surface profiles and corresponding scanning laser acoustic micrographs for sintered silicon carbide specimens.

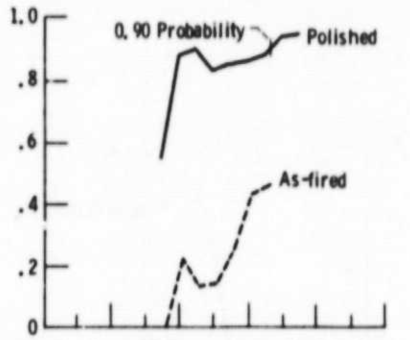

(a) Specimen thickness, approximately 4 mm.

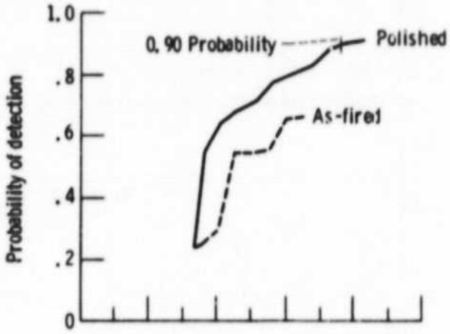

(b) Specimen thickness, approximately 3 mm.

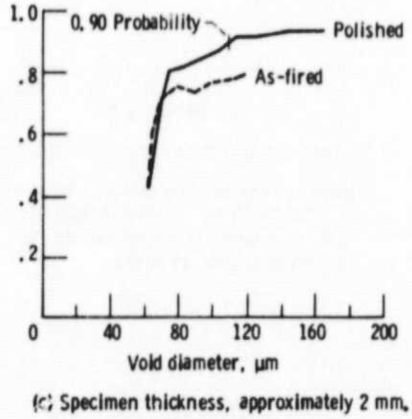

(c) Specimen thickness, approximately 2 mm.

Figure 8. - Probability of detection for voids in sintered silicon nitride specimens showing improvement in void detectability after hand polishing. Probability of detection calculated at 0.95 confidence level.

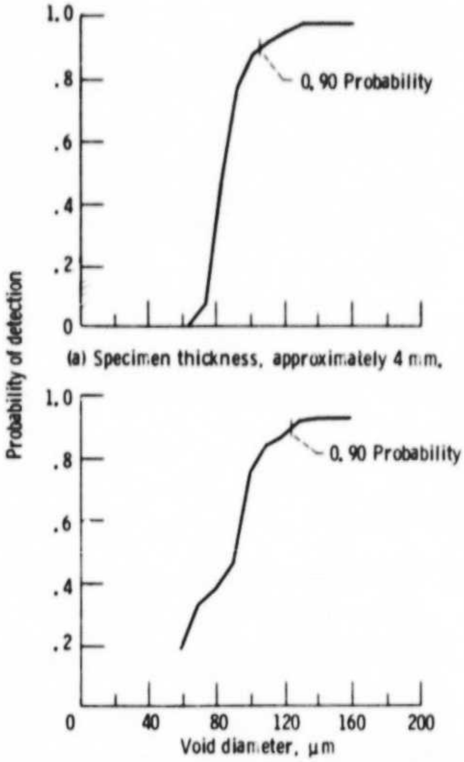

(b) Specimen thickness, approximately 3 mm.

Figure 9. - Probability of detection for voids in as-fired sintered silicon carbide specimens. Probability of detection calculated at 0.95 confidence level.

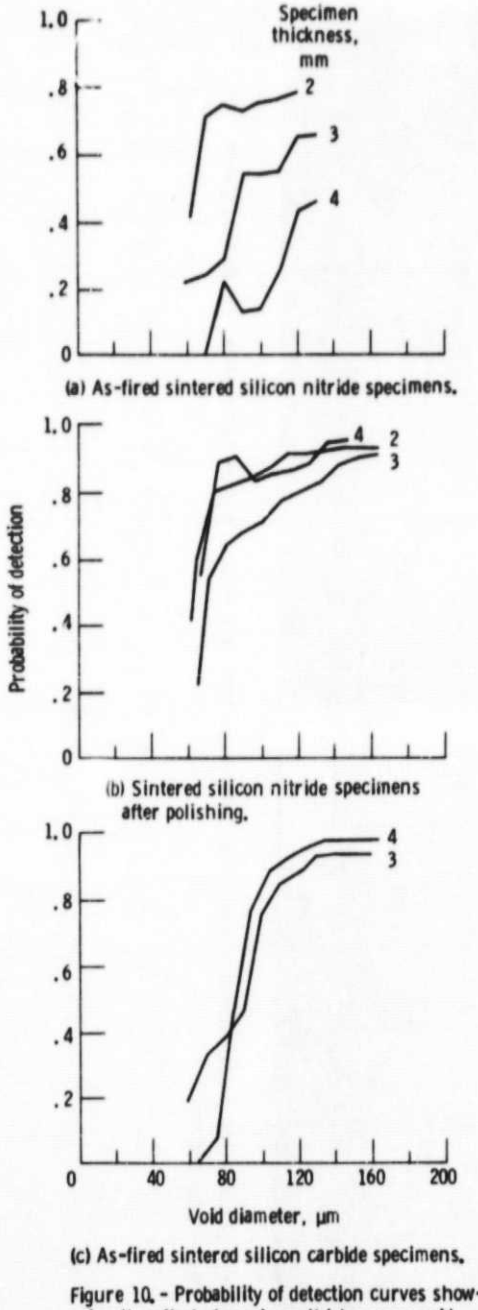

Figure 10. - Probability of detection curves showing the effect of specimen thickness on void detectability. Probability of detection calculated at a 0.95 confidence level.

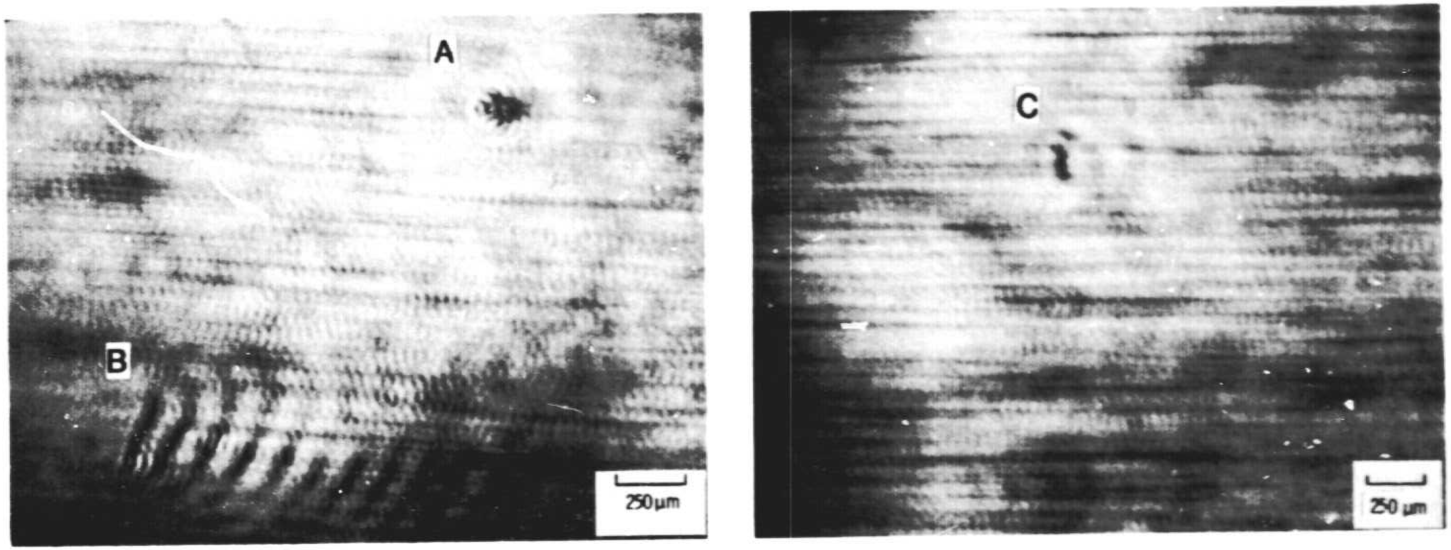

Figure 11. - SLAM micrographs illustrating images of two surface-connected flaws (A and B) and near-surface flaw (c) in diamond-ground silicon nitride specimen.

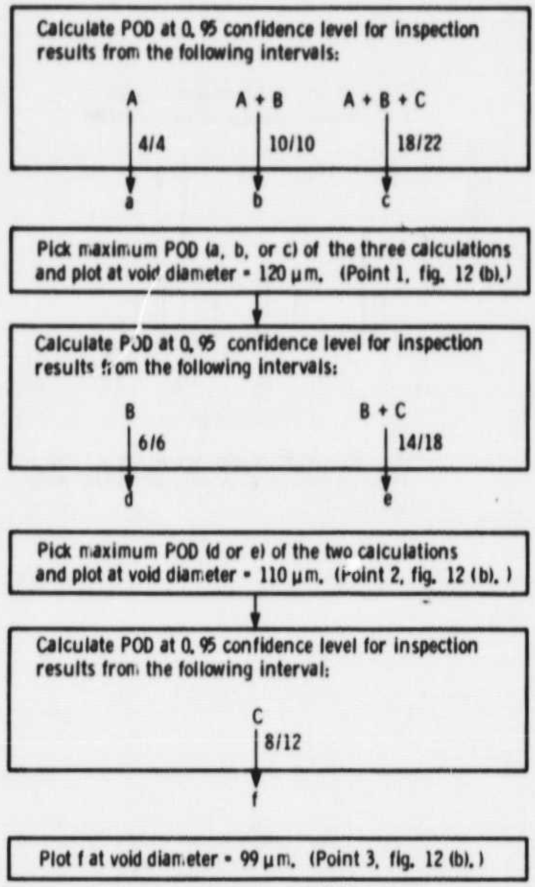

(a) Steps of optimized-probability method.

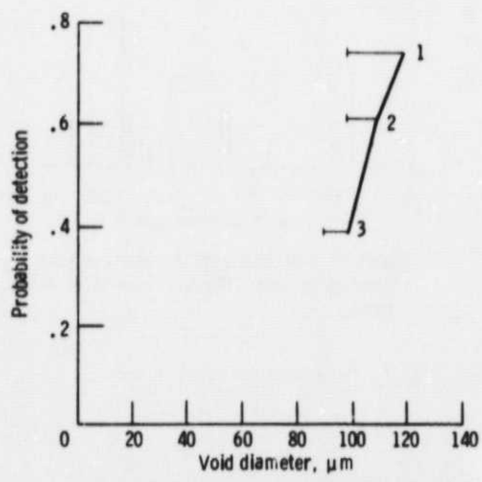

(b) Plot of probability of detection as function of void diameter generated by using optimized-probability method. Bars adjacent to data points indicate range of void diameters over which POD was calculated.

Figure 12. - Schematic of steps and plot of results of optimized-probability method using data from table II.

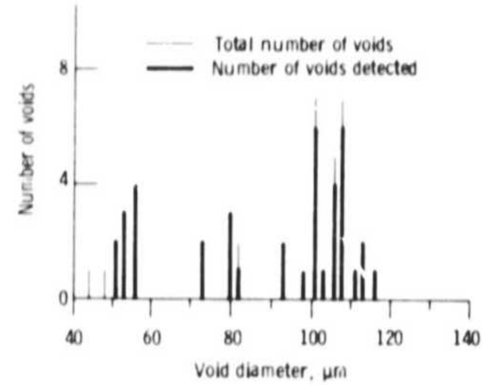

Figure 13. - As-fired SSN specimens of 2 mm nominal thickness (39 voids detected/45 voids total).

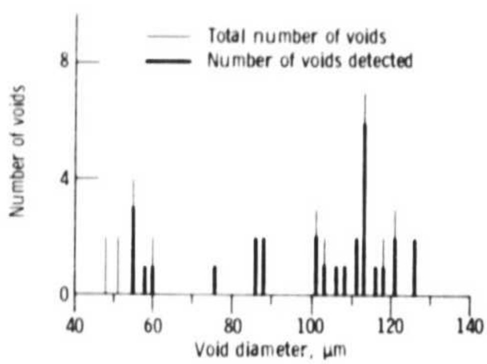

Figure 14. - As-fired SSN specimens of 3 mm nominal thickness (29 voids detected/40 voids total).

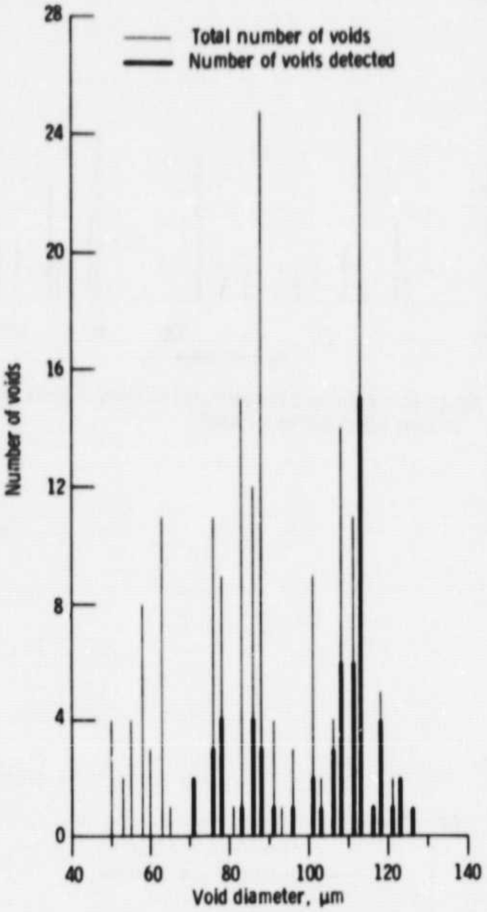

Figure 15. - As-fired SSN specimens of 4 mm nominal thickness (61 voids detected/199 voids total).

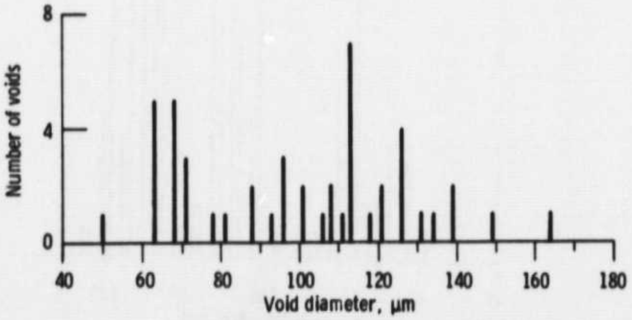

Figure 16. - Polished SSN specimens of 2 mm nominal thickness (48 voids detected/48 voids total).

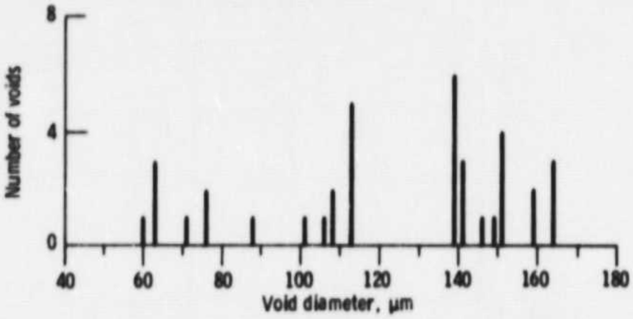

Figure 17. - Polished SSN specimens of 3 mm nominal thickness (37 voids detected/37 voids total).

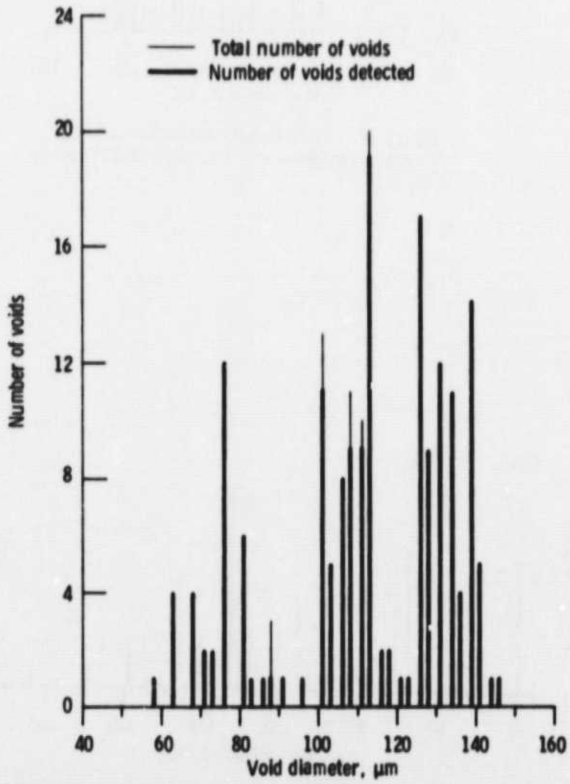

Figure 18. - Polished SSN specimens of 4 mm nominal thickness (177 voids detected/185 voids total).

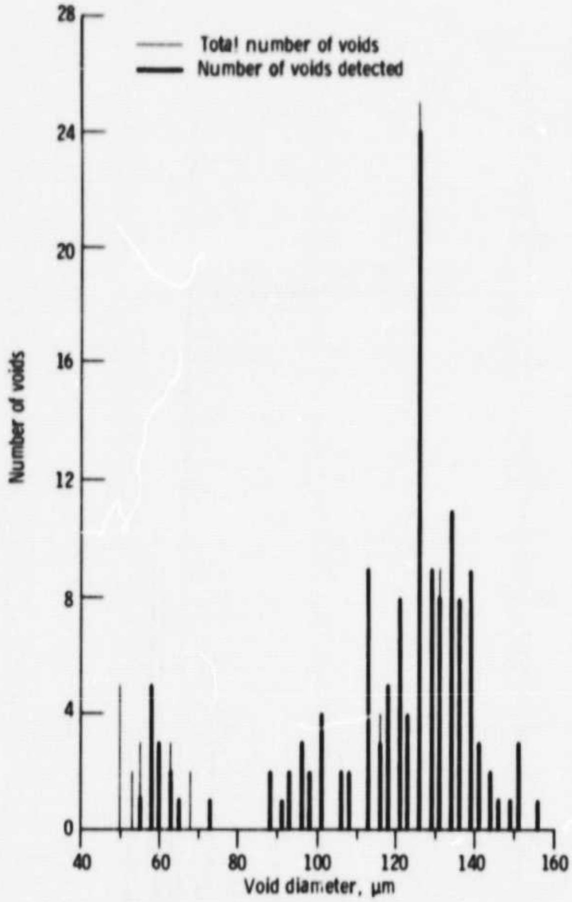

Figure 19. - As-fired SSC specimens of 3 mm nominal thickness (140 voids detected/155 voids total).

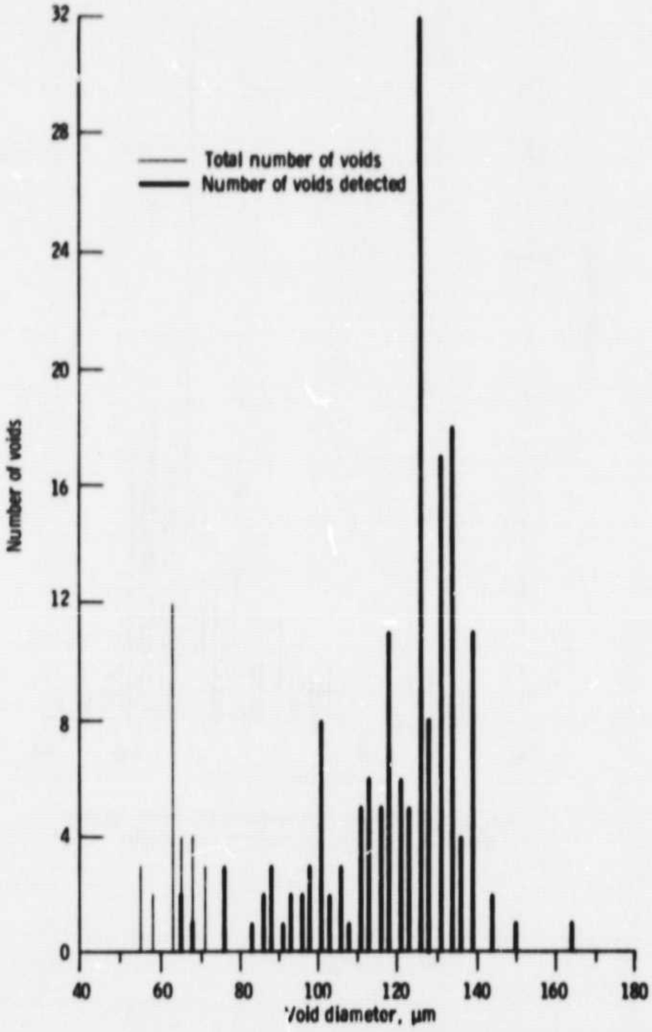

Figure 20. - As-fired SSC specimens of 4 mm nominal thickness (166 voids detected/191 voids total).

1. Report No.	2. Government Accession No.	3. Recipient's Catalog No.
NASA TM-87035		

4. Title and Subtitle	
Reliability of Void Detection in Structural Ceramics Using Scanning Laser Acoustic Microscopy	5. Report Date May 1985
	6. Performing Organization Code 506-53-1A
7. Author(s) Don J. Roth, Stanley J. Klima, and James D. Kiser, NASA Lewis Research Center, and George Y. Baaklini, Cleveland State University, Cleveland, Ohio	8. Performing Organization Report No. E-2591
	10. Work Unit No.
9. Performing Organization Name and Address National Aeronautics and Space Administration Lewis Research Center Cleveland, Ohio 44135	11. Contract or Grant No.
	13. Type of Report and Period Covered Technical Memorandum
12. Sponsoring Agency Name and Address National Aeronautics and Space Administration Washington, D.C. 20546	14. Sponsoring Agency Code

15. Supplementary Notes

Don J. Roth, Stanley J. Klima, and James D. Kiser, NASA Lewis Research Center; George Y. Baaklini, Cleveland State University, 1983 E. 24th St., Cleveland, Ohio. Prepared for the Spring Meeting of the American Society for Nondestructive Testing, Washington, D.C., March 11-14, 1985.

16. Abstract

The reliability of scanning laser acoustic microscopy (SLAM) for detecting surface voids in structural ceramic test specimens was statistically evaluated. Specimens of sintered silicon nitride and sintered silicon carbide, seeded with surface voids, were examined by SLAM at an ultrasonic frequency of 100 MHz in the as-fired condition and after surface polishing. It was observed that polishing substantially increased void detectability. Voids as small as 100 μm in diameter were detected in polished specimens with 0.90 probability at a 0.95 confidence level. In addition, inspection times were reduced up to a factor of 10 after polishing. The applicability of the SLAM technique for detection of naturally occurring flaws of similar dimensions to the seeded voids is discussed. A Fortran program listing is given for calculating and plotting flaw detection statistics.

17. Key Words (Suggested by Author(s))	18. Distribution Statement
Nondestructive testing; Ultrasonics; Acoustic microscopy; Ceramics; Voids; Flaws; Probability; Statistics	Unclassified - unlimited STAR Category 38

19. Security Classif. (of this report)	20. Security Classif. (of this page)	21. No. of pages	22. Price*
Unclassified	Unclassified		

*For sale by the National Technical Information Service, Springfield, Virginia 22161